Revised submission, Ms. ID: NCOMMS-23-41238B

Astrocytes modulate neuronal development by S100A6 signaling

Valentina Cinquina[1], Alán Alpár[2], Predrag Kalaba[3], Daniela Calvigioni[1,$], Evgenii O. Tretiakov[1], Fabiana Piscitelli[4], Erik Keimpema[1], Vincenzo Di Marzo[4,5], Alexej Verkhratsky[6,7] and Tibor Harkany[1,8,§]

[1]Department of Molecular Neurosciences, Center for Brain Research, Medical University of Vienna, Vienna, Austria,
[2]SE NAP Research Group of Experimental Neuroanatomy and Developmental Biology, Department of Anatomy, Histology, and Embryology, Semmelweis University, Budapest, Hungary,
[3]Institute of Biological Chemistry, Faculty of Chemistry, University of Vienna, Vienna, Austria,
[4]Endocannabinoid Research Group, Institute of Biomolecular Chemistry (ICB), National Research Council (CNR), Pozzuoli, Italy,
[5]Canada Excellence Research Chair on the Microbiome-Endocannabinoidome Axis in Metabolic Health, Institut Universitaire de Cardiologie et de Pneumologie de Québec and Institut sur la Nutrition et les Aliments Fonctionnels, Centre Nutriss, Université Laval, Québec, QC, Canada,
[6]Faculty of Biology, Medicine and Health, The University of Manchester, Manchester, United Kingdom,
[7]Achucarro Centre for Neuroscience, IKERBASQUE, Basque Foundation for Science, Bilbao, Spain,
[8]Department of Neuroscience, Biomedicum 7D, Karolinska Institutet, Solna, Sweden.

[$]*Present address*: Department of Neuroscience, Biomedicum 4B, Karolinska Institutet, Solna, Sweden.

[§]*Correspondence* should be addressed to **Tibor Harkany** (Tibor.Harkany@meduniwien.ac.at).

Abstract

Neuronal morphogenesis relies on intercellular signaling. Astrocytes release metabolites, trophic, and guidance factors to promote neuronal maturation. In contrast, the mechanisms by which astrocytes could limit and stabilize neuronal connectivity remain less explored. Here, we show cortical astrocytes to express and release S100A6, a Ca^{2+}-binding protein ('calcyclin'). Simultaneously, the majority of cortical neurons express calcyclin-binding protein (CaCyBp), a *bona fide* binding partner for S100A6. In neurons, CaCyBp maintains the unfolded protein response pathway, thereby controlling proteostasis. When released, S100A6 inhibits CaCyBp-mediated signaling, thus slowing protein turnover, and, consequently, neuritogenesis. S100A6-CaCyBp signaling during gestation and lactation is sensitive to the mother's nutritional status, particularly eicosapentaenoic acid intake. Thus, a member of the S100 protein family acts as an astroglia-derived morphogen, whose action on neurons is modulated by environmental factors.

Key words: calcyclin | calcyclin-binding protein | morphogenesis | cerebral cortex | intercellular communication | UPR pathway.

Introduction

Reciprocal communication with astrocytes underpins the development, survival, and excitability of neurons. Therein, astrocytes release gliotransmitters (such as canonical neurotransmitters, adenosine/ATP, and trophic factors), neurotransmitter precursors (glutamine, L-serine), and metabolites (chiefly lactate and pyruvate), and also clear excess neurotransmitters and waste products, including potential neurotoxins[1]. During brain development, astrogliogenesis coincides with synaptogenesis[1]. Astrocytes are broadly known to express and release differentiation and survival factors (e.g., brain-derived neurotrophic factor, glial cell line-derived neurotrophic factor, thrombospondin, hevin/Sparcl1) to promote the polarization, morphological differentiation, and synaptogenesis of neuroblasts[1]. In contrast, astrocyte-derived factors that are inhibitory to neuritogenesis, thus acting to balance growth *vs*. synapse selection and stabilization, remain less explored.

Considering that major steps of cellular differentiation are regulated by Ca^{2+} signals (be this the activation of kinases, cytoskeletal instability, directional growth decisions, synaptogenesis)[1], Ca^{2+}-binding and sensor proteins appear particularly important considering that some can even undergo regulated release to support intercellular interactions[2]. In astrocytes, S100β, a Ca^{2+}-binding protein within the EF-hand superfamily, is best known as one of the 25 members of the S100 protein family[2] because it is constitutively expressed in most astrocytes across brain regions[3,4], and associated with inflammation in adults[3,5]. However, if S100 proteins are expressed in astrocytes during brain development and could be assigned to regulate neuronal morphogenesis remains unknown.

Here, we explored the developmental expression patterns of S100 family proteins by processing open-label single-cell RNA-seq data during mouse fetal brain development, and identified S100A6/calcyclin, its binding partner (calcyclin-binding protein; CaCyBp), and the main downstream targets *Siah1/Siah2*, E3 ubiquitin ligases, whose expression is timed during neuritogenesis and synaptogenesis in the late

embryonic/neonatal period. We then used *in situ* hybridization and immunohistochemistry to map S100A6 and CaCyBp to astrocytes and neurons, respectively, identified S100A6 as a secreted ligand by mass spectrometry, protein biochemistry, and neurochemistry in cellular models *in vitro*, and combined genetic and pharmacological tools to demonstrate that S100A6 inhibits neuritogenesis by slowing protein turnover. Notably, we found both S100A6 and CaCyBp expression to be sensitive in the developing fetal nervous system to maternal nutrition, particularly to eicosatetraenoic acid (EPA) availability. Subsequently, we have associated the deregulation of S100A6-CaCyBp signaling between astrocytes and neurons with maternal exposure to hypercaloric/ω3-polyunsaturated fatty acid (PUFA)-enriched diets. Cumulatively, these data suggest that S100A6 is a gliotransmitter affecting neuronal morphogenesis, at least in the mouse brain.

Results

S100 proteins in the developing mouse brain

First, we addressed the expression sites and developmental dynamics of S100 proteins in the mouse brain by processing open-label single-cell RNA-seq data on the fetal somatosensory cortex[6]. During corticogenesis (that is, from embryonic day (E)10 to postnatal day (P)4), cell identities were mapped in age-matched tissues by UMAP representation (**Fig. 1a-d**). Progenitors, as well as astrocytes were subdivided into 16 clusters based on marker gene expression (*see Methods*; **Fig. 1d**). Fifteen of the S100 proteins were detected from E10.5 on (**Fig. 1e**). Four of the proteins (S100A1, S100A6, S100A13, and S100A16) gradually increased in expression in astrocytes (up to P4). Among these, *S100a6* (also termed 'calcyclin') showed a sharp increase between E18.5 and P4, when astrogliogenesis peaks[1,6] (**Fig. 1e**). Detailed examination of the gene sets conferring cell identity in the single-cell RNA-seq data showed that S100A6 is specifically expressed by astrocytes in neonatal and postnatal mouse neocortex (**Fig. 1f,g; Supplementary Fig. 1a**). As such, UMAP representation revealed that *S100a6* expression matched with astrocytes also enriched in e.g., *S100b*[7], *Apo4*[8], *and Aldh1l1*[9,10] (**Supplementary Fig. 1b**). qPCR and Western blotting validated the presence of *S100a6* mRNA (n = 4-7 male mice/time point, p = 0.003 for E14.5 *vs.* P4, one-way ANOVA followed by Tukey's multiple comparisons test) and protein expression (n = 3 male mice/time point; p = 0.017 for E18.5 *vs.* P4, Student's *t*-test), respectively, during development (**Supplementary Fig. 1c,d**). These data suggest that S100A6 could specifically control a hitherto unknown event during brain development, noting that its expression can be maintained in mature astrocytes postnatally[11].

S100A6 and calcyclin-binding protein localization

S100A6 promotes cell proliferation and differentiation, and protects from noxious insults[12,13]. S100A6 contains two EF-hand Ca^{2+}-binding motifs, which are helix-loop-helix structural domains (**Supplementary Fig. 1e**). Upon Ca^{2+} binding, S100A6 undergoes a conformational change that exposes a hydrophobic region to allow for its interaction with target proteins. Chiefly, S100A6 binds to the C-terminus of calcyclin-binding protein (*Cacybp* or *S100a6bp*) to promote its interaction with *Siah1a/Siah1b*, E3 ubiquitin ligases, through its N-terminal domain (**Supplementary Fig. 1f**). Thus, S100A6, if released from astrocytes, may regulate protein degradation/turnover in neighboring cells, including neurons, alike in other tissues[14,15], and malignant cells[7].

Single-cell RNA-seq placed *Cacybp* in both apical progenitors and postmitotic neurons (**Fig. 1e,h,i**; **Supplementary Fig. 1g**). When testing the availability of *Cacybp* in neurons, we found it ubiquitously expressed at E10.5, with stable levels from E14.5 to P4 (**Fig. 1e,h**; **Supplementary Fig. 1g**). *Siah1a* and *Siah1b* were also detected by single-cell RNA-seq (**Fig. 1e**). At E18.5, when *S100a6* starts to increase in the astrocyte lineage (**Fig. 1e,g**), UMAP assigned *Cacybp* expression to virtually all neuronal lineages in the mouse neocortex (note its limited expression in astrocytes for cell-autonomous function; **Fig. 1i**). CaCyBp expression at both the mRNA and protein levels was confirmed by qPCR (**Supplementary Fig. 1h**; n = 5-7 male mice/time point, p = 0.009 for E14.5 *vs*. P4, one-way ANOVA followed by Tukey's multiple comparisons test) and Western blotting (**Supplementary Fig. 1i;** n = 3 male mice/time point, p = 0.040 for E18.5 *vs*. P4, Student's *t*-test). Both methods demonstrated stable levels of *Cacybp* mRNA and CaCyBp protein during development, followed by a significant increase postnatally.

Complementarity of S100A6 and calcyclin-binding protein expression

To map S100A6 and CaCyBp in brain tissue, we performed *in situ* hybridization experiments on coronal sections of E18.5 and P4 mouse brains (n = 3 male mice/time point) using probes specific for these markers (*see* Methods). In the somatosensory cortex (ssCtx; **Fig. 2a**), co-localization between *S100a6* and *S100b*[7], *Apoe*[8], *Aldh1l1*[9,10], and *Gfap* mRNAs, pleiotropic markers of astrocytes, was found along the cortical plate (cp) at both E18.5 and P4 (**Fig. 2a,d**; **Supplementary Fig. 2**).

During the same developmental window, *Cacybp* expression was chiefly confined to cells that co-expressed the neuronal marker *Rbofox3* (which encodes NeuN; **Fig. 2b,e; Supplementary Fig. 3a,b**; n = 3 male mice/time point throughout). The neuronal identity of *Cacybp*$^+$ cells was further confirmed by immunohistochemistry, showing CaCyBp expression in both excitatory and inhibitory neurons in the ssCtx of mice at both E18.5 and P4 (**Fig. 2c,f**; **Supplementary Fig. 3c,d**). At E18.5, 96.3% of the cells that populated the ssCtx co-expressed both CaCyBp and microtubule-associated protein (MAP2), a neuronal marker. Moreover 17.0% of neurons were positive for both CaCyBp and calretinin (CR, **Fig. 2c** *upper*; **Supplementary Fig. 3c,d**; n = 3 male mice/time point). Similar results were found at P4, when 90.8% of cells co-labelled for CaCyBp$^+$/MAP2$^+$ and 19.1% for CaCyBp$^+$/CR$^+$ (**Fig. 2c** *bottom*; **Supplementary Fig. 3c,d**; n = 3 male mice/time point). Likewise, CaCyBp was observed in the somatodendritic axis of neurons in the cortical plate of human fetuses during the second trimester (**Fig. 3a**; gestational week (GW) 27; male subject). Similar results were obtained in the adult cerebral cortex of both mice (**Supplementary Fig. 3e**; P120; male) and humans (**Supplementary Fig. 3f**; age: 60 years, male subject).

We then used primary cell cultures enriched in either neurons or astrocytes to support the cell-type-specific enrichment of both *S100a6* and *Cacybp* (**Supplementary Fig. 3g**; n = 3-5 biological replicates mixed for sex). The *S100a6*:*Cacybp* mRNA (**Fig. 3b**) and protein (**Fig. 3c**) ratios were ~15:1 in astrocytes, whereas ~1:18 in neurons Thus, we reveal the mutually exclusive expression of *S100a6* and *Cacybp* in astrocytes *vs*. neurons during corticogenesis, and suggest that intercellular S100A6-to-CaCyBp signaling could constitute a novel mode of intercellular communication with S100A6 acting as a *bona fide* gliotransmitter.

S100A6 is released from astrocytes

For S100A6 to be classified as an astrocyte-derived ligand, its expression shall be regulated (e.g., by neurotransmitters and neuromodulators) and undergo activity-dependent release. We tested these properties *in vitro*, aided by IncuCyte-assisted live-cell imaging to control cell viability, by exposing primary astrocytes to glutamate (100 μM) for up to 24 h. Glutamate triggered S100A6 accumulation in the culture medium, with a ~4-fold increase by 24 h (**Fig. 4a**; n = 3 biological replicates; mixed for sex; p = 0.044 0 h *vs*. 6 h; p < 0.0001 0 h *vs*. 24 h, p = 0.001 6 h *vs*. 24 h; one-way ANOVA followed by Tukey's multiple comparisons). We propose this to be regulated S100A6 release given the lack of cell death (**Fig. 4b; Supplementary Fig. 4a**; *see* Methods for the 3-(4,5-Dimethylthiazol-2-yl)-2,5-diphenyltetrazolium bromide (MTT) assay and statistics), and the parallel (albeit disproportionate) increase in cytosolic S100A6 levels (within 6 h; **Supplementary Fig. 4b**; p = 0.021 0 h *vs*. 2 h; p = 0.012 0 h *vs*. 6 h; one-way ANOVA followed by Bonferroni's multiple comparison; n = 6 biological replicates, mixed for sex).

Next, we asked if S100A6 could bind to CaCyBp by exposing Neuro-2a cells, which were invariably CaCyBp$^+$ (**Supplementary Fig. 4c**), to His-tagged recombinant S100A6 (1 μg/μl; 'pulse-chase experiment'). After 1 h, His-S100A6 was detected intracellularly in Neuro-2a cells by super-resolution microscopy (**Fig. 4c**). LC-MS/MS analysis supported these findings by detecting trypsin-cleaved peptide fragments specific to S100A6 in treated but not control Neuro-2a cultures (**Fig. 4d; Supplementary Fig. 4d,e**). Overall, these findings suggest a transcellular action analogous to those of trophic factors and morphogens[16], wherein astroglia could serve as a source of S100A6 regulating neuronal responses by CaCyBp-based ligand recognition[17].

S100A6 limits neuronal morphogenesis

We tested this hypothesis by exposing cortical neurons to recombinant S100A6 (1 μg/μl) for 4 days, which significantly reduced neurite complexity (**Fig. 4e**; n = 3 biological replicates; mixed for sex; p = 0.003; Student's t-test). This morphogenetic response coincided with reduced CaCyBp protein levels (**Fig. 4f**; n = 3 biological replicates; mixed for sex; p = 0.005; Student's t-test), which we qualified as a desensitization response. We then knocked down *Cacybp* expression in primary cortical neurons by AAV-mediated shRNA transduction. Attenuated *Cacybp* expression (at 15 days *in vitro*; **Supplementary Fig. 4f—h**) reduced neurite outgrowth relative to mock-transfected controls (**Fig. 4g;** n = 23-27 cells; mixed for sex; p < 0.001 *vs*. mock-transfected controls; Student's t-test).

We then combined *Cacybp* knock-down with exposure to recombinant S100A6 (1 μg/μl) 24 h later. qPCR analysis showed an additive effect on both *Tubb3* (**Fig. 4h;** n = 5-8; mixed for sex; p = 0.045 [sh*Cacybp*] *vs*. [control]; p = 0.048 [His-S100A6] *vs*. [control]; p = 0.002 [sh*Cacybp* + his-S100A6] *vs*. [control]; one-way ANOVA followed by Tukey's multiple comparison; ANOVA summary: F = 6.757; p = 0.0016) and *Actb* (**Fig. 4h;** n = 9-7; mixed for sex; p = 0.027 [sh*Cacybp*] *vs*. [control]; p = 0.008 [His-S100A6] *vs*. [control]; p = 0.005 [sh*Cacybp* + his-S100A6] *vs*. [control]; one-way ANOVA followed by Tukey's multiple comparison; ANOVA summary: F = 6.226; p = 0.0022) following CaCyBp downregulation. Moreover, immunocytochemistry followed by single-cell reconstruction showed a reduction in neurite length (including the longest

one designated as the putative 'axon') after treatment (**Fig. 4j** 'axon': $p < 0.0003$ [sh*Cacybp*] *vs*. [control]; $p = 0.003$ [His-S100A6] *vs*. [control]; $p = 0.002$ [sh*Cacybp* + his-S100A6] *vs*. [control]; ANOVA summary: F = 11.88; $p = 0.0004$; **Fig. 4j** neurites: $p = 0.0102$ [sh*Cacybp*] *vs*. [control]; $p = 0.004$ [His-S100A6] *vs*. [control]; $p = 0.023$ [sh*Cacybp* + his-S100A6] *vs*. [control]; one-way ANOVA followed by Tukey's multiple comparison; ANOVA summary: F = 7.16; $p = 0.0038$). The total number of neurites was not affected (**Fig. 4i**). These data identify a role for S100A6 in limiting neuritogenesis through CaCyBp[14,18] (**Fig. 4k**).

Neuritogenesis relies on the rapid expansion of the cytoskeleton, and its enrichment in specific proteins (receptors, transporters) along the neurite axis, including the prospective synapse. Subcellular fractionation placed CaCyBp in the cytosol, in particular in the endoplasmic reticulum (ER; **Fig. 5a**). Electron microscopy confirmed this localization with CaCyBp often found in the proximity of the cisternae of the ER of neurons (**Fig. 5b**; **Supplementary Fig. 5a**). This location suggested that CaCyBp could be poised to affect proteostasis[19] (that is, protein synthesis and/or turnover at the ER).

CaCyBp modulates protein turnover in neurons

Cortical neurons after *Cacybp* knock-down had reduced protein content (*vs*. mock transfected cells; **Fig 5c**; $n = 4$ male mice; $p = 0.005$ *vs*. [mock-transfected control]; Student's *t*-test). Therefore, we tested the expression of molecular constituents of the ER stress pathway, whose activation increases protein degradation[20] by serving as effectors of the unfolded protein response (UPR) machinery[19]: G-protein coupled receptor 78 (*Grp78;* $p = 0.001$), cyclic AMP-dependent transcription factor ATF-6 alpha (*Atf6a;* $p = 0.008$), unspliced X-box-binding protein 1 (*Xbp1u;* $p < 0.001$) and spliced X-box-binding protein 1 mRNAs (*Xpi1s;* $p = 0.002$) were all downregulated (**Fig. 5d**; $n = 6$ biological replicates; mixed for sex; Student's *t*-test). This suggests the absence of a first phase (acute) cellular response to restore protein homeostasis. Besides cellular imaging (**Fig. 4g—j**), we used CCAAT-enhancer-binding protein homologous protein (CHOP)[21] as a surrogate to show that attenuated *Cacybp* expression did not trigger pro-apoptotic signaling (**Fig. 5d**; $p = 0.701$).

Subsequently, we tested the expression of ubiquitin specific peptidase 9, X-linked (USP9X) and ubiquitin specific peptidase 7 (USP7), both acting as deubiquitinating enzymes to prevent protein degradation by the proteasome[22], and thus being instrumental for cellular survival and function[23]. USP9X levels were significantly decreased (**Fig. 5e;** $p = 0.008$ *vs*. [mock-transfected control], $n = 3$ biological replicates; mixed for sex; Student's *t*-test). USP7 showed lesser reduction (**Fig. 5e;** $p = 0.113$ *vs*. [mock-transfected control]; $n = 3$ biological replicates). These results were compatible with increased tubulin acetylation (**Fig. 5f**; $p < 0.001$ *vs*. [mock-transfected control]; $n = 3$ biological replicates; mixed for sex; Student's *t*-test), a post-translational mark of long-lived microtubules, suggesting slowed cytoskeletal dynamics[24,25]. These changes were phenocopied by sustained exposure to recombinant S100A6, which similarly reduced *Cacybp* expression (**Supplementary Fig. 5b—f**).

Subsequently, we asked if treating neurons with another S100 family member, S100A4, which was also expressed by astrocytes during brain development, even if more sporadically, (**Fig. 1e**; **Supplementary Fig. 6a**) could mimic the morphogenetic effects of S100A6. It is noteworthy that a binding partner for S100A4 is not known, and CaCyBp does not bind S100A4[26]. S100A4 exposure did not affect neurite

development *in vitro* (**Supplementary Data Fig. 6b**). Similarly, the expression of neither *Cacybp* nor of the molecular constituents of the ER stress pathway were altered (**Supplementary Fig. 6c**).

Lastly, we asked if S100A6 localization within Neuro-2a cells could be affected by shRNA-mediated *Cacybp* knock-down. To this end, Neuro-2a cells were transfected with siRNA targeting *CaCyBp* for 96 h, with subsequent exposure to His-tagged S100A6 for an additional 1 h. Super-resolution microscopy (**Fig. 5g**) revealed S100A6 intracellularly. This is not unexpected because CaCyBp does not represent a cell-surface binding site that would limit S100A6 internalization. Yet we found reduced S100A6 localization within the ER fraction where CaCyBp would physiologically accumulate (**Fig. 5h**). Thus, we outline an intracellular signaling cascade centered on the UPS machinery for astrocyte-derived S100A6 to limit neuronal morphogenesis (*see also* **Fig. 4k**).

S100A6 signaling is sensitive to eicosapentaenoic acid

Next, we sought to address if environmental factors, particularly components of a maternal diet that is societally seen as 'healthy' could affect S100A6-CaCyBp signaling in the developing brain. We hypothesized that eicosapentaenoic acid (EPA), an ω-3 polyunsaturated fatty acid (PUFA) that is particularly enriched in experimental diets (**Supplementary Table 1**), could be a candidate to affect S100A6 signaling because it modulates both neurogenesis [27,28] and astrocyte differentiation[29] by being incorporated in the membranes of glial cells[29-31]. However, a biological substrate for EPA is as yet unknown.

First, we tested the dose-dependence of EPA action on both neurons and astrocytes. By using high-throughput live-cell imaging of neurons for 7 days, we found that 1 μM but not 5 μM concentrations of EPA induced neuritogenesis in cortical neurons (including branching; **Fig. 6a;** n = 7 biological replicates; mixed for sex; neurite length: $p < 0.0001$ [control] vs. [EPA 5 mM], $p < 0.0001$ [EPA 1 mM] vs. [EPA 5 mM]; neurite branches: $p < 0.0001$ [control] vs. [EPA 5 mM], $p < 0.0001$ [EPA 1 mM] vs. [EPA 5 mM]; two-way ANOVA followed by Tukey's multiple comparisons) without adversely affecting neuronal viability (**Supplementary Fig. 7a**). EPA did not impact astrocyte proliferation even at an excessive dose of 30 μM after 24 h (**Fig. 6b; Supplementary Fig. 7b**). No effect was seen on astrocyte viability either (**Supplementary Fig. 7c**). Yet, EPA increased the metabolic activity of astrocytes in the MTT assay (**Supplementary Fig. 7c**), which we interpreted as altered mitochondrial function likely upstream to ER stress[32]. Then we asked if EPA could be one of the effectors to modulate S100A6 secretion from astrocytes particularly since increased cellular metabolism could underpin release events. Thus, we exposed astrocytes to EPA (30 μM) for 24 h and we found that it induced S100A6 release *in vitro* (**Fig. 6c**; $n = 3$ biological replicates; mixed for sex; $p < 0.0001$ [0 h] *vs*. [24 h], $p = 0.0004$ [6 h] *vs*. [24 h]; one-way ANOVA followed by Tukey's multiple comparisons). Both 5 μM and 10 μM EPA concentrations were also effective (**Supplementary Fig. 7d**). Thus, we characterized S100A6 as a gliotransmitter possibly released upon EPA exposure, at least *in vitro*.

Next, we performed experiments in which conditioned media of astrocytes, collected 6 h after EPA exposure (30 μM), were transferred onto neurons (**Supplementary Fig. 7e**). After an incubation period of 24 h, neurons treated with conditioned media had reduced *Cacybp* mRNA levels (**Fig. 6d**; $n = 3$ biological replicates; mixed for sex; $p = 0.021$; Student's *t*-test), as well as a lowered expression of the molecular constituents of the ER stress pathway (**Fig. 6e**; $n = 3$ biological replicates; mixed for sex) *in vitro*.

Thereafter, we sequentially knocked down S100A6 expression in astrocytes by a pool of siRNAs (1 μM) for 96 h, exposed them to EPA (30 μM) for 6 h, and then collected conditioned media for transfer onto neurons (for 24 h; **7a**) to specify astrocyte-derived S100A6 as a mediator of EPA-induced growth effects on neurons. In astrocytes, both Western blotting (cytosol) and ELISA (medium) revealed attenuated S100A6 expression upon EPA treatment relative to either mock-transfected controls or EPA alone (**Fig. 7b,c,c1**). In neurons, standard culture medium and astrocyte-conditioned medium (conditioning for 6 h only without treatment to the astrocytes; **Supplementary Fig. 8a**) led to a statistically significant increase in neuronal growth (**Supplementary Fig. 8b**). This effect is compatible with neuronal differentiation in response to growth factors released by astrocytes. From this point on, the morphological variables determined in neurons exposed to conditioned astrocyte medium served as baseline ('control'). In addition, we used direct stimulation by EPA (30 μM; **Fig. 7a**) to limit bias through its direct effect as 'left-over contaminant' in conditioned media after 6 h. Once depleting conditioned media in S100A6 by RNAi, neurons underwent neuritogenesis (no mock-transfected controls at this point; **Fig. 7d,e**; p = 0.042 [control] *vs*. [sRNA alone]). Moreover, a differential, and statistically significant, neuritogenic response was observed when comparing EPA alone that reduced the length of the lead neurite *vs*. siRNA-mediated *S100a6* knockdown in conjunction with EPA stimulation (p = 0.0006 [conditioned with EPA] *vs.* [siRNA + conditioned with EPA] (one-way ANOVA followed by Tukey's multiple comparisons). Likewise, the cumulative length of neurites and their branching were rescued when knocking down *S100a6* before conditioning astrocytes with EPA (neurite length: **Fig. 7f,** *left***;** p = 0.0005 [conditioned with EPA] *vs.* [siRNA + conditioned with EPA]; branching: **Fig. 7f,** *right***;** p = 0.0001 [control] *vs*. [sRNA alone], and p = 0.025 [conditioned with EPA] *vs.* [siRNA + conditioned with EPA]; one-way ANOVA followed by Tukey's multiple comparisons). As before, increase S100A6 levels in the conditioned medium were coupled with a reduction of *Cacybp* mRNA expression in neurons (**Supplementary Fig. 8c**). Thus, we suggest that modulating S100A6 release from astrocytes ultimately impinges upon neuronal differentiation through CaCyBp engagement.

Transgenerational modulation of S100A6 signaling

EPA is a key component of 'ω-3 polyunsaturated fatty acid (PUFA)-enriched' diets in humans, which are preferred during pregnancy[33,34]. Therefore, we exposed female dams for 8 weeks to a hypercaloric diet enriched in ω-3 PUFAs prior to conception and throughout pregnancy (**Supplementary Fig. 9a**; **Supplementary Table 1**)[35] (EPA enrichment: ~ 5-fold *vs.* control diet).

We first analyzed the cytoarchitectonic features of fetal cortices at E18.5 after gestational exposure to the experimental diet. Wild-type C57Bl6/J dams were pulsed with 5-ethynyl-2'-deoxyuridine (EdU) on E14.5, the peak of cortically-oriented neurogenesis[36], with the distribution of EdU^+ progeny in fetal cortices quantified and plotted on E18.5 (**Fig 8a**). The total number of EdU^+ cells did not differ between the groups (224 ± 9 cells/mm^2 [experimental diet] vs. 363 ± 14 cells/mm^2 [standard diet]; p = 0.199; **Supplementary Fig. 9b**). In contrast, the distribution of EdU^+ cells across cortical laminae, which were separated by their different cellular packing densities[35,37], were dissimilar, with an increased density of EdU^+ cells at the deep cortical plate-subplate boundary (*layer 5*: 12 ± 1 cells/mm^2 [experimental diet] vs. 7 ± 0 cells/mm^2 [standard diet]; p = 0.003; *layer 6*: 4 ± 0 cells/mm^2 [experimental diet] vs. 3 ± 0 cells/mm^2 [standard diet]; p = 0.026), as well as the subventricular zone (*layer* 9: 15 ± 2 cells/mm^2 [experimental

diet] vs. 10 ± 2 cells/mm^2 [standard diet]; $p = 0.028$; **Fig 8a**). Conversely, the uppermost cortical plate/marginal zone that forms first in the outside-in hierarchy of cortical lamination [38] had lesser EdU$^+$ cells (*layer 2*: 4 ± 1 cells/mm^2 [experimental diet] vs. 13 ± 2 cells/mm^2 [standard diet]; $p = 0.016$; **Fig 8a**). These data suggest the layer-specific redistribution of postmitotic neuroblasts from equivalent pools of progenitors in the fetal brain when dams receive the experimental diet, causing an imbalance in their metabolites.

Moreover, we observed an ~45% decrease in the expression of growth-associated protein 43 (GAP43; $n = 3$ male mice/group; $p = 0.018$ *vs.* [standard diet]; Student's *t*-test), and ~65% reduction in microtubule-associated protein 2 (MAP2; $n = 3$ male mice/group; $p < 0.0001$ *vs.* [standard diet]) along the fetal somatosensory cortex (**Supplementary Fig. 9c,d**), indicating a potential dysregulation of cortical neurogenesis during embryonic development. This decrease was also validated by iTRAQ methodology[24] ($n = 3$ mice/group; mixed for sex) allowing the unbiased testing if protein contents were affected by the experimental diet. Among the 266 proteins whose levels changed in the fetal cortices at E18.5 (129 *vs*. 137 proteins being up- or down-regulated; **Supplementary Table 2**), both GAP43 and MAP2 were found reduced in the brains of male fetuses in a gene ontology cluster identified as '*structural activity/cytoskeleton*' (**Fig. 8b,c**). Moreover, we found 18 proteins (7%) of the cluster '*proteasome*' and 48 proteins (18%) of '*translation, ribosome assembly, endoplasmic reticulum*' changed (**Fig. 8b**), providing faithful coverage of the proteostasis network[39]. Within the '*proteasome*' cluster, CaCyBp was particularly reduced (**Fig. 8c;** male mice) and correlated with increased S100A6 levels. Western blotting corroborated the iTRAQ data (**Fig. 8d;** $n = 3$ male mice/group; $p = 0.003$ *vs.* [standard diet]; $p < 0.0001$ *vs.* [standard diet]; Student's *t*-test). We have also detected reduced total protein content in fetal cortices (**Fig. 8e**; $n = 3$ male mice/group; $p = 0.01$ *vs.* standard diet; Student's *t*-test) and increased tubulin acetylation (**Fig. 8f**; $n = 3$ male mice/group; $p = 0.002$) after gestational exposure to the experimental diet.

Finally, we have assessed if key parameters of cortical reorganization endure into the adulthood of offspring prenatally exposed to an experimental diet. We particularly focused on anxiety-like behaviors because of the prevalence of this endophenotype upon manipulations with dietary PUFAs[35]. In the elevated plus-maze paradigms, we determined a significant reduction of entries in the open arms (**Fig. 8g;** $p = 0.023$). Cumulatively, these data suggest that S100A6-CaCyBp signaling is sensitive to manipulation of dietary PUFA levels during pregnancy, its activity affects corticogenesis *in vivo*[23], with a life-long manifestation of depression-like behaviors in adult offspring.

Discussion

Astrocytes and neurons communicate through an array of fundamental mechanisms during brain development, each playing a crucial role in forming a functional nervous system[40]. As a prototypical signalling axis, brain-derived neurotrophic factor (BDNF), alike other neurotrophins and growth factors, is known to be released by astrocytes to support neuronal survival, growth, and differentiation[1,41]. Ca^{2+} signalling is another essential mechanism, where astrocytes use protracted Ca^{2+} rises to release gliotransmitters like ATP/adenosine, modulating both neuronal activity and synaptic transmission[42].

Among the numerous signalling molecules involved, the S100 protein family plays a significant role[43]. These Ca^{2+}-binding proteins can at as sensors (that is, to recruit partner proteins intracellularly to initiate

signalling cascades) to modulate, e.g., cell proliferation, differentiation, and response to injury[44]. Specifically, S100A6/calcyclin influences neurodevelopment by regulating cytoskeletal dynamics, and cell survival[18,45,46]. Through these actions, S100A6, when focally released by astrocytes in an activity-dependent fashion, might facilitate the proper alignment, synaptogenesis, and wiring of neurons, ensuring the accuracy of connectivity in the developing brain.

Here, we described a molecular signalling pathway priming astrocyte-to-neuron interactions. Stimulation of astrocytes can lead to S100A6 release. S100A6 then could bind CaCyBp on the cell surface or intracellularly. Our study is limited in addressing if and how free S100A6 could be internalized, which is likely given that CaCyBp knock-down did not curtail intracellular S100A6 accumulation. Yet we note that CyCyBp is not a cell-surface receptor but a sensor protein adjoining the ER, and henceforth transport and targeting mechanisms ought to exist for its S100A6 through the plasma membrane and cytosolic enrichment, respectively. Notwithstanding, an ensuing shift in the activity of the ubiquitin-proteasome system (UPS), a pathway fundamental for protein degradation, likely dampens cellular processes that are at the peak of their activity during neuronal growth and development[19]. Particularly, slowed protein turnover could then reduce cytoskeletal instability, leading to, e.g., reduced neuritogenesis.

S100A6-CaCyBp signalling appears to be a molecular pathway sensitive to eicosapentaenoic acid (EPA), a key ω-3 fatty acid that has anti-inflammatory and neuroprotective properties[27,28,31,47]. During pregnancy, ω-3 fatty acids play a crucial role in fetal brain development[48,49]. In particular, EPA aids the formation of neuronal membranes, enhances membrane fluidity, and ensures the efficient transmission of neural signals[47]. EPA also influences gene expression to facilitate the growth and differentiation of neurons, including synaptogenesis, and myelination[50,51]. Thus, ensuring adequate ω-3 fatty acid intake during pregnancy, including EPA, is essential for physiologically-adequate fetal brain development, being the foundation for cognitive and neurological health throughout life. We found that a hypercaloric experimental diet enriched in ω-3 fatty acids altered cortical architecture (that is, the number, positioning and molecular composition of neurons), as shown by the reduced expression of both GAP43 and MAP2. This phenotype was associated with an increase in S100A6, and a concomitant reduction in CaCyBp, corroborating *in vitro* results. These changes could also be linked to an altered status of the UPS, alike cells were either treated with S100A6 or CaCyBp silenced by RNAi. It is of note, that many cytoarchitectural changes seen at late-gestation became alleviated during postnatal life, yet an anxiety-like phenotype remained. This is not entirely unexpected since polyunsaturated fatty acid (PUFA) imbalance, whether due to the dominance of ω-6 or ω-3 PUFAs[35], can affect exploratory behaviors in stressful environments, at least in laboratory rodents. Thus, we suggest that EPA-enriched diets can influence fetal brain development through the modulation of S100A6-CaCyBp signaling between astrocytes and neurons, potentially imposing long-lasting modifications to intercellular signaling that can compromise resilience to environmental challenges later in postnatal life.

In conclusion, our results describe a novel molecular axis of astrocyte-neuron communication, which is unique in limiting neuronal morphogenesis through the ER/UPS pathway. By using S100A6 as a released ligand, astrocytes can define endpoints of neuronal morphogenesis, particularly neuritogenesis. Therefore, S100A6 could be recognized as an astrocyte-specific gliotransmitter, which acts through a signaling cascade centered on the regulation of neuronal proteostasis.

Acknowledgements

We thank J. Mulder and M. Uhlén (Kaarolinska Institutet) for anti-S100A6 and anti-CaCyBp antibodies, G.G. Kovacs (Medical University of Vienna) for human tissues, and S.L. Shirran, C.H. Botting (University of St. Andrews, United Kingdom), M.A. Fuszard (Martin-Luther University, Germany), P. Poullet (Institut Curie & INSERM U900, France) for iTRAQ proteomics and analysis; P. Kalaba and A. Fabisikova (from Mass Spectrometry Center; Univerity of Vienna) for LC-MS/MS. This work was supported by the Austrian Science Fund (P 34121-B; E.K.), the National Brain Research Program of Hungary (2017-1.2.1-NKP-2017-00002, NAP2022-I-1/2022; A.A.), the Excellence Program for Higher Education of Hungary (TKP-EGA-25; A.A.), the Swedish Research Council (T.H.); Novo Nordisk Foundation (T.H.); Hjärnfonden (T.H.), the European Research Council (FOODFORLIFE, 2020-AdG-101021016; T.H.), and an intramural research grant of the Medical Neuroscience Cluster of the Medical University of Vienna (2021-1; T.H.).

Author contributions

T.H. conceived the project. V.C., V.D.M., A.V. and T.H. designed experiments. T.H. procured funding. V.C., D.C., F.P., and E.K. performed *in vivo* and *in vitro* experiments and analyzed data. A.A. contributed electron microscopy data. P.K. performed mass-spectrometry-based ligand identification. E.O.T. performed and supervised single-cell data analysis. V.C. and T.H. wrote the manuscript with input from all co-authors.

Conflict of interest

The authors declare that they have no conflict of interest.

Data availability

iTRAQ data are being deposited in PRIDE with the accession number becoming available by final acceptance.

Supplementary Information is available in the online version of the paper.

Code availability

The code developed and used in this report has been published at https://harkany-lab.github.io/Cinquina_2024. A whole system setup was also made available for download. Data analysis using Bootstrap-coupled Estimation were also deposited (https://harkany-lab.github.io/Cinquina_2024/methods.html).

Corresponding author statement

Correspondence and requests for materials should be addressed to T.H. (tibor.harkany@ki.se or tibor.harkany@meduniwien.ac.at).

Online methods

Animals and ethical approval of *in vivo* studies

Female mice (C57Bl6/J) were housed in groups (5 mice/group) in perplex cages on a 12h/12h light/dark cycle (lights on at 08:00 h) and in a temperature (22 ± 2 °C) and humidity (50 ± 10%)-controlled environment. Food and water were available *ad libitum*. Embryos and tissues were obtained from timed matings with the day of vaginal plug considered as embryonic day (E) 0.5. Group sizes were defined as per conventions in developmental biology[35,52]. Experiments on live animals conformed to the 2010/63/EU European Communities Council Directive and were approved by the Austrian Ministry of Science and Research (66.009/0277-WF/V/3b/2017). Particular effort was directed towards minimizing the number of animals used and their suffering during experiments.

Single-cell RNA sequencing data analysis

We analyzed single-cell RNA sequencing data from developing mouse cortex spanning embryonic day (E) 10 to postnatal day (P) 4. The dataset was obtained from Ref.[6], and accessed through the Single Cell Portal (SCP1290)[53]. Raw count data and metadata were downloaded and processed using Seurat (v5.1.0) in R (vR version 4.4.0 (24/04/2024))[54,55]. We chose Seurat for its comprehensive toolset for quality control, analysis, and exploration of single-cell RNA-seq data, as well as its wide adoption in the field.

Data preprocessing and quality control: The raw count matrix was loaded using the '*Read10X function*' in Seurat. We performed the following pre-processing steps: *i*) the log1p normalized matrix was converted back to raw counts by applying '*expm1*'; *ii*) scaling factors were calculated based on the total UMI counts/cell. The count matrix was scaled by multiplying each cell's counts by its scaling factor; *iii*) a new Seurat object was created using the scaled count matrix; *iv*) cells annotated as doublets, low quality, or red blood cells were removed using the '*subset*' function; *v*) data were then normalized using the '*NormalizeData*' function, and 5,000 highly variable features were identified using '*FindVariableFeatures*'.

Dimensionality reduction and clustering: We performed principal component analysis (PCA) on variable features using '*RunPCA*'. Based on the Elbow plot, which indicates the variability of each principal component (PC), we selected the first 30 out of 50 PCs for downstream analysis. This choice helped us to reduce noise in the data while ensuring biological reproducibility of the results. Uniform Manifold Approximation and Projection (UMAP) [56] and *t*-distributed Stochastic Neighbor Embedding (t-SNE)[57,58] were used for dimensionality reduction, with embeddings stored in the Seurat object. Both techniques used the selected 30 PCs as input. Cells were clustered using the '*FindNeighbors*' and '*FindClusters*' functions. For community detection, we employed the Leiden algorithm (resolution = 0.7) instead of the commonly used Louvain algorithm or alternatives such as walktrap, multilevel, or infomap. The Leiden algorithm was chosen for its ability to find converged optimal solutions more efficiently, which is particularly beneficial for large-scale single-cell datasets[59].

Gene expression analysis: We analyzed the expression of S100 family genes and a curated list of genes of interest across different developmental stages and cell types. Feature plots, violin plots, and dot plots

were generated using Seurat's visualization functions ('*FeaturePlot*', '*VlnPlot*', '*DotPlot*') and custom functions from the scCustomize package (v2.1.2).

Analysis of the astrocyte lineage: Cells annotated as astrocytes, apical progenitors, and cycling glial cells were subset for focused analysis of the astrocyte lineage. This subset was re-clustered using the same approach as above. We performed differential expression analysis between astrocyte clusters using both the '*FindAllMarkers*' function in Seurat (using a logistic regression test[60]) and DESeq2 (v1.44.0)[61] on pseudo-bulk data aggregated by cluster and developmental stage. The combination of these two approaches allowed us to leverage the strengths of both single-cell and bulk RNA-seq differential expression methods. Data preprocessing, quality control (including droplet selection, ambient RNA removal, doublet detection, and refined filtering), clustering, marker gene definitions, and the specific software packages used for data processing were made available at https://harkany-lab.github.io/Cinquina_2024/cortex_visualisation.html.

Human tissue, immunohistochemistry

Fetal brains (gestational week (GW) 27; *n* = 3 samples; mixed for sex) were collected at the Neurobiobank of the Institute of Neurology, Medical University of Vienna, Austria. Tissues were obtained and used in compliance with the Declaration of Helsinki and following institutional guidelines approved by the Ethical Committee of the Medical University of Vienna (No. 396/2011). Fetal brain tissue was obtained from spontaneous or medically induced abortions. Fetuses whose cause of death was unrelated to genetic disorders, head injury, neurological diseases, or other known diseases (e.g., infections) were only included. Tissues were kept at 4 °C for 24–48 h due to local regulations before immersion fixation in formalin (10%) on average for 34–37 days before embedding in paraffin. Three-µm tissue sections of formalin fixed, paraffin-embedded tissue blocks were mounted on pre-coated glass slides (StarFrost). Following deparaffinization and rehydration, sections were incubated in a solution of H_2O_2 (3%) and MeOH (Millipore; Catalog #: 67_56_1) for 10 min to block endogenous peroxidase activity. After washing with distilled water, sections were pre-incubated in low pH EnVision™ FLEX antigen retrieval solution (PTLink; Dako) at 98 °C for 20 min, exposed to fetal calf serum (10%) for 10 min and subsequently stained with rabbit anti-CaCyBp antibody (**Supplementary Table 3**) at 4 °C for 72 h. The EnVision detection kit (K5007, ready-to-use, DAKO) was used to visualize the horseradish peroxidase/DAB reaction product with H_2O_2 substrate (0.01%). Sections were counterstained with hematoxylin-eosin, dehydrated in an ascending series of ethanol, cleared with xylene and covered with Consil-Mount (Thermo Scientific), and viewed under a light microscope (Nikon Eclipse E400). We did not observe variations in the cellular distribution of CaCyBp across the samples. Therefore, a representative image was included.

Immunohistochemistry, light and electron microscopy in mice

Adult male mice were transcardially perfused with ice-cold 0.1 M PB (20 ml), followed by 4% PFA in PB (100 ml at 3 mL/min flow speed). P120 adult brains were post-fixed in 4% PFA overnight. After equilibrating in 30% sucrose for 48–72 h, coronal serial sections (1-in-6 series) were cryosectioned (Leica CM1850) at a thickness of 50 µm. Free-floating sections were processed as described[62] for either fluorescence microscopy or chromogenic (using 3,3'-diaminobenzidine (DAB) as substrate) electron microscopy. E18.5

and P4 brain were immersion fixed in 4% PFA overnight, rinsed in PB, and cryoprotected in 30% sucrose (in PB) for 48 h. Serial coronal sections (20 µm) were cut, thaw-mounted onto fluorescence-free Super-Frost$^+$ glass slides, and stored at −20 °C until processing.

For fluorescence histochemistry, E18.5, P4 and P120 sections from *n* = 4 male mice were extensively rinsed in PB, and blocked with PB containing 5% normal donkey serum (NDS; Jackson ImmunoResearch; Catalog #: 017000121), 1% bovine serum albumin (BSA; Sigma; Catalog #: A2153), and 0.3% Triton X-100 (Sigma) at 21-24 °C for 2 h to reduce non-specific labeling. Next, sections were incubated with a combination of primary antibodies (**Supplementary Table 3**) diluted in PB also containing 2% NDS, 0.1% BSA and 0.3% Triton X-100 at 4 °C for 72 h. DyLight Fluor 488, 560, or 633-tagged secondary antibodies (1:300; Jackson ImmunoResearch) were used for signal detection. Hoechst 33,342 (Sigma; Catalog #: B2261) and 4',6-diamin-2-phenylindol (DAPI, Sigma) were routinely used as nuclear counterstains. After washing in PB and a final rinse in distilled water, free-floating sections were mounted onto fluorescence-free glass slides and coverslipped with Mowiol mounting medium. Fluorescence images were acquired on a Zeiss 880 LSM confocal laser-scanning microscope equipped for maximal signal separation and spectral scanning/unmixing.

Electron microscopy was performed as previously published[23]. Briefly, free-floating sections from male adult mice were washed three times with PB for 5 min each and then treated with 1% H_2O_2 (Sigma; Catalog #: 216763) for 10 min to block endogenous peroxidase activity. After rinsing, sections were exposed to a blocking solution (*see above*) at 21-24 °C for 2 h. Sections were then incubated with a rabbit anti-CaCyBp primary antibody (**Supplementary Table 3**) for 72 h. After washing three times, sections were exposed to biotinylated anti-rabbit secondary antibodies (1:200; Jackson ImmunoResearch, 20–22 °C, 2 h), rinsed again in PB, and then exposed to preformed avidin-biotin-peroxidase complexes (1:200, ABC Elite; Vector Laboratories; Catalog #: PK6100) at 4 °C overnight. Next, biotin-labeled cells were revealed using a peroxidase reaction with DAB alone (5 mg/ml, 0.03% H_2O_2 as substrate, brown reaction product). Sections were subsequently osmificated (1% OsO_4 in PB, 15 min), dehydrated in an ascending ethanol gradient followed by flat embedding in Durcupan (FLUKA, ACM). Ultrathin sections (60 nm) were cut on a Leica ultramicrotome, collected on Formvar-coated single slot grids, and analyzed with a Tecnai 10 electron microscope (FEI; primary magnifications: 6200x; 17500x).

In situ hybridization (HCR-FISH)

Fresh-frozen E18.5 and P4 mouse brains were cryosectioned at a thickness of 16 µm and collected on SuperFrost$^+$ glass slides (ThermoFisher). Sections were immersed in 4% PFA for 15 min, and dehydrated in an ascending ethanol gradient (50%, 70%, and 100%; 5 min each). The HCR™ RNA-FISH protocol for either fresh-frozen or fixed-frozen tissue sections (Molecular Instruments) was used with pre-designed *Cacybp*, *S100a6*, *Rbfox3*, *Gfap*, *S100b*, *Aldh1l1*, *and Apo4* probes. Samples were imaged on an LSM 880 confocal microscope (Zeiss) at 40× primary magnification.

Neuronal cultures, shRNA knockdown, treatment with recombinant S100A6

588 Cerebral tissues (cortex/hippocampus) of mouse embryos (mixed for sex) were isolated on either E18.5
589 or P0. Cells were mechanically dissociated into a single-cell suspension by papain digestion (20 U/ml, pH
590 7.4, 45 min; Worthington, #LK003176) and plated onto poly-D-lysine-coated (PDL; Sigma; #P728) 6-well
591 (200,000 cells/well) or 24-well (50,000 cells/well) plates. Cells were maintained in Neurobasal medium
592 (Fisher Scientific; #10888_022) supplemented with B27 (1%; Thermo Fisher; #17504-044), GlutaMAX™
593 (1%; ThermoFisher; #35050_038), and penicillin/streptomycin (1%; Life Technologies; #15140_122). Me-
594 dia were replaced every other day.
595
596 For shRNA knock-down of *Cacybp*, P0 cortical neurons (200,000 cells/well) were seeded in 6-well plates,
597 grown for 48 h, then transduced with either 1 µl of adeno-associated virus, serotype 2 (AVV-2) particles
598 (6.09 x 10^{12} genome copies/ml; GeneCopoeia™; #AA02-CS-MSE091282-AVE001-01-200) to carry shRNA
599 or equal amounts of AVV-2s to deliver scrambled controls (GeneCopoeia™; #AA02-CS-CSECTR001-
600 AVE001-01-200). Media were replaced with Neurobasal medium (*as above*) free of AAV-2 particles after
601 48 h, and changed every other day. Alternatively, P0 neurons in 6-well plates were exposed to either 1 µg
602 of recombinant His-tagged S100A6 protein (Abcam; #ab108124) or 1 µg of recombinant His-tagged
603 S100A4 protein (Abcam; #ab109341) for 24 h on DIV14. Analyses of neuronal morphology were per-
604 formed on 15 DIV because *Cacybp* mRNA and protein levels were found significantly reduced by then in
605 shRNA-exposed samples *vs*. both technical controls and samples treated with scrambled shRNA. Cells
606 were then lysed for Western blotting and qPCR after 15 days *in vitro* (DIV). Morphometric analysis of
607 cultured neurons was aided by the ImageJ software and included the length of the primary neurite (µm).
608
609 In combined experiments, P0 neurons were plated in 6-well plates (200,000 cells/well), while E18.5 neu-
610 rons in glass bottom dishes (25,000 cells/well; 35 mm diameter, 20 mm well size; 0.13-0.16 mm bottom;
611 Cellvis, #D35-20-1-N). Cells were grown for 48 h, then transfected with AVV-2 particles as above. After 14
612 DIV, neurons were exposed to 1 µg of recombinant His-tagged S100A6 protein for 24 h. Neurons in 6-well
613 plates were then processed for RNA extraction and qPCR. Neurons in glass-bottom dishes were immer-
614 sion-fixed in 4% PFA (in 0.1 M phosphate-buffered saline [PBS]) for 1 h, and then exposed to a blocking
615 solution consisting of 10% NDS, 5% BSA, and 0.3% Triton X-100 in PBS (pH 7.4) at 21-24 °C for 2 h. To
616 visualize F-actin, cultured neurons were incubated with Alexa Flour 546-conjugated phalloidin (1:500;
617 Invitrogen; **Supplementary Table 3**) for 2 h. Hoechst 33,342 (Sigma; #B2261) was routinely used as nuclear
618 counterstain.
619
620 To test the effects of astrocytes (with/without genetic manipulation; *see below*), E18.5 neurons were
621 plated first in 24-well plates (50,000 cells/well), 96-well plates (20,000 cells/well for morphometry) or 6-
622 well plates (1x10^6 cells/well for qPCR), and allowed to grow until 3 DIV. At this point, half of the neuronal
623 media was replaced with either fresh neuronal media or astrocyte-conditioned media for another 24 h.
624 Neuronal morphology and gene expression were then analyzed.
625
626 For S100A4 treatment, E18.5 neurons were plated at a density of 50,000 cells/well on glass bottom dishes
627 (*as above*). After 3 DIV, neurons were exposed to 1 µg of recombinant His-tagged S100A4 protein (Abcam;
628 #ab109341) for 24 h. Cells were then immersion-fixed in 4% PFA, and incubated in a blocking solution for
629 2 h (*as above*). Subsequently, samples were exposed to a guinea pig anti-MAP2 primary antibody

(**Supplementary Table 3**) diluted in PBS also containing 2% NDS, 0.1% BSA and 0.3% Triton X-100 at 4 °C for 24 h. DyLight Fluor 488-tagged secondary antibody were used to visualize MAP2 localization.

After rinsing the samples in PBS and finally in distilled water, coverslips were mounted onto fluorescence-free glass slides using Mowiol. Images were acquired on a Zeiss 880LSM confocal laser scanning microscope with maximal signal separation and spectral scanning/unmixing.

High-throughput neurite tracking

Mouse cerebral cortices were isolated on E18.5. Cells were mechanically dissociated and plated at a density of 20,000 cells/well in PDL-coated 96-well plates for on-line morphometry. After 24 h, E18.5 cultures were exposed to either recombinant S100A6 (1 μg/ml; Abcam #ab108124) for 4 DIV or EPA (either 1 μM or 5 μM; Cayman, #90165) for 7 days. Before use, EPA was flushed with N_2, then dissolved in DMSO. Aliquots were stored in glass amber vials at −20 °C until needed. Working concentrations of the EPA stock solution were diluted as appropriated to achieve the necessary final concentration in neuronal media containing BSA as antioxidant.

Treatment was in quadruplicate and imaged live using an IncuCyte Zoom high-throughput device (Sartorius). Time-lapse images were acquired in loops with 2-h intervals. The growth rate of neurites in each well was obtained by measuring the surface area covered by neurites and expressed as mm/mm^2 surface area. Surface occupancy of the neurons after wither 4 DIV or 7 DIV in culture was computed as the percentage surface area covered by live neurons ('*body cluster area*'), and considered as a measure of cell survival.

Primary culture of astrocytes, confluence analysis, and S100A6 secretion

Cortices and hippocampi of P7 mice (n = 7) were isolated, dissociated into single cell suspension by papain (*as above*), and plated in T75 flasks. Cells were maintained in DMEM (high glucose, 1% GlutaMAX™; Thermo Fisher, #61965_026) supplemented with Na-pyruvate (1%; Sigma #11360_070), fetal bovine serum (FBS; 10%, Sigma, #A5256801) and 1% penicillin/streptomycin. After 7–9 days, T75 flasks were placed on a shaker (180 rpm, 37 °C, overnight) to remove cell debris, neurons, and oligodendrocytes.

For confluence analyses, astrocytes were plated at a density of 7,000 cells/well into 96-well plates. After 24 h, astrocytes were placed in serum-free medium for 24 h, and then treated with glutamate (100 μM; Tocris, #56_86_0) and EPA (5, 10 and 30 μM; Cayman, #90110) for another 24 h. Before use, glutamate was dissolved in sodium hydroxide, EPA was flushed with N_2, dissolved in dimethyl sulfoxide, its aliquots stored at −20 °C, and used as above. Glutamate and EPA treatments were performed in quadruplicate and imaged live using an IncuCyte Zoom high-throughput imaging device (Sartorius). Time-lapse images were acquired every 2 h. Confluence was determined as above.

To detect S100A6 secretion, astrocytes (1×10^6) were trypsinated (0.25% trypsin-EDTA, Gibco, #25200_56), and seeded in 6-well plates. After 24 h, astrocytes were starved in serum-free medium at 37 °C for 24 h, and then treated with either glutamate (100 μM) or EPA (5, 10, and 30 μM) for an additional

673 24 h. Supernatants were collected and concentrated using either Amicon Ultra-4 centrifugal units (3kDa
674 cut-off; Sigma, #UFC800324) by centrifugation at 7,500 *g* for 40 min or Amicon Ultra-0.5 centrifugal units
675 (3kDa cut-off; Sigma #UFC500396) by centrifugation at 14,000 *g* for 30 min. Concentrated supernatant
676 was then used to detect S100A6 by Western blotting and/or an ultrasensitive mouse anti-S100A6 ELISA
677 (antibodies-online.com; ABIN425090)[63] as per the manufacturer's protocol. Astrocytes were pelleted,
678 lysed, and used for Western blotting.
679
680
681 **siRNA-mediated knockdown, astrocyte-conditioned medium on neuros**
682 To knock-down S100A6 expression, astrocytes were plated at a density of 300,000 cells/well in 12-well
683 plates. After 24 h, astrocytes were placed in serum-free medium for 24 h. S100A6 expression was silenced
684 by siRNA (1 μM; Dharmacon, #SO-3248729G). Scrambled siRNA (1 μM; Dharmacon, #D-001950-01-50)
685 was used as control. Cells were lysed and collected for Western blotting after 96 h. To benchmark this
686 manipulation, S100A6 protein was significantly reduced in siRNA-exposed samples *vs*. both technical con-
687 trols and samples treated with scrambled siRNA (**Fig. 7**). After RNAi-mediated S100A6 silencing, astrocytes
688 were treated with EPA (30 μM) for 6 h, when their pellets and supernatants were collected for Western
689 blotting.
690
691
692 **MTT assay**
693 The 3-(4,5-dimethylthiazol-2-yl)-2,5-diphenyltetrazolium bromide colorimetric assay was carried out at
694 the end of each IncuCyte run to determine drug effects on the viability of astrocytes. MTT (Abcam;
695 #ab146345) was added to each well at a final concentration of 0.5 mg/ml, incubated for 3 h, with the
696 medium then aspirated. One hundred μl of 100% DMSO (Sigma; #472301) was then added to each well.
697 After the formazan crystals had dissolved, absorbance was determined spectrophotometrically at 570 nm.
698 Data on astrocyte viability were analyzed using 'Data analysis using Bootstrap-coupled estimation
699 (DABEST; package v2023.9.12) in *R* for effect sizes and their confidence intervals[64] (*see also*:
700 https://harkany-lab.github.io/Cinquina_2024/methods.html).
701
702
703 **Neuro-2a cells, transfection, immunocytochemistry**
704 Neuro-2a cells (CCL-131, ATCC) were kept in DMEM (high glucose, 1% GlutaMAX™, ThermoFisher,
705 #61965_026) supplemented with 1 % Na-pyruvate, 10 % FBS, and 1% penicillin/streptomycin. Neuro-2a
706 cells were trypsin dissociated every 4th day, and newly passaged cells were used in experiments 24-48 h
707 after re-plating. Neuro-2a cells were directly lysed in either Laemmli buffer (for Western blotting; Bio-
708 Rad, #1610747) or RNA extraction medium (for qPCR), or used for immunoprecipitation (*see below*).
709
710 *Immunocytochemistry on Neuro-2a cells*: For immunocytochemistry, cells were plated at a density of
711 50,000 cells/well in 24-well plates. After 24 h, cells were exposed to recombinant S100A6 (1 μg/μl; Abcam,
712 #ab108124;) for 1 h, immersion-fixed in 4% PFA (in 0.1 M PBS), and exposed to a blocking solution con-
713 sisting of 10% NDS, 5% BSA, and 0.3% Triton X-100 in PBS (pH 7.4) at 21-24 °C for 2 h. Next, samples were
714 incubated with rabbit anti-S100A6 primary antibody (**Supplementary Table 3**) diluted in PBS also contain-
715 ing 2% NDS, 0.1% BSA and 0.3% Triton X-100 at 4 °C for 24 h. Alexa Flour 546-conjugated phalloidin (1:500;

716 Invitrogen; **Supplementary Table 3**) and DyLight Fluor 488-tagged secondary antibody (1:300; Jackson
717 ImmunoResearch) were used for F-actin and S100A6 signal detection, respectively. Hoechst 33,342
718 (Sigma, #B2261) was routinely used as nuclear counterstain. After washing in PBS and a final rinse in dis-
719 tilled water, coverslips were mounted onto fluorescence-free glass slides with Mowiol. Images revealing
720 the subcellular localization of S100A6 were acquired on a Zeiss 880LSM confocal laser scanning micro-
721 scope with maximal signal separation and spectral scanning/unmixing.
722
723 For the subcellular localization of S100A6, Neuro-2a cells were plated at a density of either 50,000
724 cells/well in 24-well plates or 10 x 10^6 cells in 10-cm Petri dishes for 24 h. Subsequently, they transduced
725 with 1 µl of AVV-2 particles for shRNA delivery (*as above*). Media were replaced with DMEM free of AAV-
726 2 particles after 48 h. After an additional 24 h, cells were exposed to recombinant S100A6 (1 µg/µl) for 1
727 h and then processed for either immunocytochemistry or subcellular fractionation (*see below*). S100A6
728 were then detected in both the cytosolic and endoplasmic reticulum fractions by ELISA (antibodies-
729 online.com; #ABIN425090) according to the manufacturer's instructions[63].
730
731
732 **Immunoprecipitation and Nano LC-MS/MS measurements**
733 Neuro-2a cells were plated at a density of 10 x 10^6 cells in 10-cm Petri dishes and exposed to recombinant
734 S100A6 (1 µg/µl) for 1 h. Total protein was extracted, and immunoprecipitation performed using HisCube
735 Ni-INDIGO His-tag MAgBeads MINI Kit according to the manufacturer's instructions. Briefly, 20 µl of Ni-
736 Beads (Cube Biotech, #75201) were transferred to 1.5 mL low-binding tubes, magnetized in a magnetic
737 rack, with the supernatant discarded. Beads were washed (3x) with 0.5 ml PB (each washing step with
738 short vortexing, spin-down, magnetizing, and discarding the supernatant). Proteins were added to washed
739 Ni-Beads and incubated at 4 °C overnight. Subsequently, samples were magnetized and washed (3x).
740 Beads were eluted (5x) by adding 30 ml imidazole (500 mM, pH 7.4), incubated for 10 min on a shaker at
741 room temperature, and magnetized. Eluents were collected and added to ice-cold acetone (1:4) and left
742 to precipitate at -20°C overnight. Precipitated protein samples were centrifugated at 14,000 *g* at 4 °C for
743 1 h, left to dry, and then solubilized in triethylammonium bicarbonate buffer (50 mM) on a shaker at room
744 temperature for 2 h. Trypsin digestion was performed at 37 °C for 16 h. Formic acid was then added to
745 the collection tubes, eluents were evaporated in a SpeedVac at 30 °C for 4 h, and processed for LC-MS.
746
747 Mass spectra were obtained using an Orbitrap Q Exactive mass spectrometer (Thermo Fisher Scientific)
748 equipped with a nanospray ion source coupled to a HPLC system (UltiMate 3000, Dionex). Five µL of each
749 sample was first loaded on a pre-column (trap column; Acclaim PepMap100, 100 µm x 2 cm, nanoViper
750 C18, 5 µm, 100 Å, Thermo Scientific) for 10 min using a loading solvent (2% acetonitrile (ACN), 98% H_2O,
751 0.1% trifluoroacetic acid) at a flow rate of 10 µl/min. Separation was carried out on a C18 analytical col-
752 umn (Acclaim PepMap RSLC, 75 µm x 50 cm, nanoViper C18, 2 µm, 100 Å; Thermo Scientific) at a flow rate
753 of 300 nL/min. Column oven temperature was kept at 40.0 °C. Mobile phase A composition was 2% ACN,
754 98% H_2O, 0.1% formic acid (FA), while mobile phase B was made up of 80% ACN, 20% H_2O, and 0.1% FA.
755 Gradient conditions were within 135 min retention time at a flow rate of 0.3 µl/min, with mobile phase B
756 set to 2%-90%. MS scans were acquired in positive ion mode over an *m/z* range of 400-1400 at a resolution
757 of 70.000 (FWHM at *m/z* 200). Using a data-dependent acquisition mode, the 6 most intense precursor
758 ions with charge states 2+ to 4+ were selected for fragmentation at 30% normalized collision energy and

759 analysed in the orbitrap at a resolution of 17.500 (at *m/z* 200). The dynamic exclusion for the selected
760 ions was 30 s. The electrospray voltage was 2.2 kV and the ion transfer capillary temperature was 300 °C.
761 Raw data were converted into mascot generic format (mgf) files using the msConvert tool from the Pro-
762 teoWizard toolkit (ProteoWizard: Home (sourceforge.io)), and subsequently processed with ProteinPro-
763 spector (version 6.5.0, University of California). Data were searched against N-terminally His-tagged
764 mouse S100A6/PRA protein sequences (Accession No. P14069, MGSSHHHHHHSSGLVPRGSHMAC-
765 PLDQAIGLLVAIFHKYSGKEGDKHLSKKELKELIQKELTIGSKLQDAEIARLMDDLDRNKDQEVNFQEYVAFLGALALIYNE
766 ALK), as well as the whole mouse proteome in the SwissProt database (version 2021), which yielded iden-
767 tical results. As further confirmation, pure recombinant S100A6/PRA protein was analyzed as standard.
768
769
770 **RNA isolation and quantitative PCR**
771 The RNeasy mini kit (Qiagen, #7326820) was used to extract RNA from mouse cerebral tissues and primary
772 cultures. DNase I was used to eliminate traces of genomic DNA. Total RNA was then reverse transcribed
773 to a cDNA library in a reaction mixture using a high-capacity cDNA reverse transcription kit (Applied Bio-
774 systems, #4368814). The cDNA library was then used for quantitative real-time PCR (CFX-connect, Bio-
775 Rad). Pairs of PCR primers specific for *Cacybp*, *S100a6*, *Grp78*, *Atf4*, *Atf6a*, *Chop*, *Xbp1u*, *Xbp1s, Map2,*
776 *Tubb3, S100b, Aldh1l1*, and *Actb* were designed with Primer Bank and the NCBI Primer Blast software
777 (**Supplementary Table 4**). Quantitative analysis of gene expression was performed with SYBR Green Mas-
778 ter Mix Kit (Life Technologies, #1725124). Expression levels were normalized to glyceraldehyde-3-phos-
779 phate dehydrogenase (*Gapdh*), a housekeeping gene, for every sample in parallel assays ($n \geq 3$ biological
780 replicates/group).
781
782
783 **Total protein determination and subcellular fractionation**
784 Total protein was extracted from cerebral tissues and primary cultures by using a modified radioimmuno-
785 precipitation assay buffer containing 5 mM NaF (Sigma, #7681_49_4), 5 mM Na_3VO_4 (Sigma,
786 #13721_39_6), 0.1% N-octyl-β-d-glucopyranoside (Sigma, #08001), and a cocktail of protease inhibitors
787 (Complete™, Roche, #11873580001). Samples were homogenized in a Dounce homogenizer, and protein
788 lysates were pelleted at 10,000 *rpm* at 4 °C for 10 min. To fractionate endoplasmic reticulum (ER) and
789 cytoplasm, samples were homogenized in 0.32 M Sucrose (Sigma, #57903); 1 mM $NaHCO_3$ (Sigma, #
790 56297), 1 mM $MgCl_2$ (Sigma, #A0344733); 0.5 mM $CaCl_2$ (Sigma, #C7902) and a cocktail of protease inhib-
791 itors and centrifuged twice at 700 *g* at 4 °C for 5 min. The supernatant was centrifuged several times to
792 collect the ER fraction (6,300 *g* at 4 °C for 10 min, 20,000 g for 30 min, and 100,000 g for 1 h). The final
793 pellet was then reconstituted as the ER fraction, whereas the supernatant was saved as the cytosol frac-
794 tion. Protein concentrations were determined by the Pierce™ BCA Protein Assay kit (Thermo Fisher,
795 #23225). Cofilin and calnexin antibodies were used to control enrichment of the cytosol and ER fraction,
796 respectively (**Supplementary Table 3**).
797
798
799 **Quantitative Western blotting, including total protein normalization**
800 Western blotting was performed with primary antibodies listed in **Supplementary Table 3**. Blots were
801 scanned on a Bio-Rad XRS⁺ imaging system and then quantified in Image Lab 3.01 (Bio-Rad). GAPDH was

802 used as loading control. For total protein normalization, labeling of the samples was initiated by carbocy-
803 anine (Cy)5 dye reagent (GE Healthcare) that had been pre-diluted (1:10) in ultrapure water. Samples
804 were mixed and incubated at 21-24 °C for 5 min. The labeling reaction was terminated by adding Amer-
805 sham WB loading buffer (GE Healthcare; 20 µl/sample) containing 40 µM dithiothreitol (Sigma,
806 #10197777001). Equal amounts of the samples (20 µg/40 µl) were boiled at 95 °C for 3 min, and then
807 loaded onto an Amersham WB gel card (13.5%). Electrophoresis (600 V, 42 min) and protein transfer onto
808 PVDF membranes (100 V, 30 min) were at default settings in an integrated Amersham WB system (GE
809 Healthcare). After blocking, membranes were incubated with primary antibodies overnight (**Supplemen-**
810 **tary Table 3**). Antibody binding was detected by species-specific Cy3-labeled secondary antibodies
811 (1:1,000; GE Healthcare). Membranes were dried before scanning at 560 nm (Cy3) and 630 nm (Cy5) ex-
812 citation. Automated image analysis was performed with the Amersham WB evaluation software with lin-
813 ear image optimization, if necessary.
814
815
816 **Prenatal exposure to an experimental diet**
817 Female C57Bl6/J animals at 6 weeks of age were randomly assigned to either a hypercaloric diet enriched
818 ~70-fold in ω-3 PUFAs or a standard diet. Prospective dams consumed the experimental diet for 8 weeks
819 prior to conception. Diets were from Special Diet Services (United Kingdom) and quality controlled by
820 mass-spectrometry (**Supplementary Table 1**). The effect of maternal nutrition on fetal brain development
821 was evaluated at E18.5[35]. Embryos were collected from $n \geq 5$ different pregnancies to keep the number
822 of independent observations sufficient for statistical analyses, sexed if appropriate, and used for histo-
823 chemistry, proteomics, and molecular biology. The use of specific or mixed genders for particular experi-
824 ments was specified throughout. Embryos were collected by Cesarean sections from mothers terminally
825 anesthetized by isoflurane (5%, 1 L/min flow rate), weighed, and decapitated with their heads either im-
826 mersed in 4% PFA in 0.1 M PB (pH 7.4) overnight or snap-frozen in liquid N_2 and stored at -80° C [52,65].
827
828
829 **Click-iT EdU labeling**
830 Dams were intraperitoneally injected ('pulsed') with 5-ethynyl-2'-deoxyuridine (EdU, 33 mg/kg) at E14.5.
831 At E18.5, n = 5 male embryos/group were selected by PCR genotyping (see Ref. [24] for primer pairs and
832 protocol). Their brains were immersion fixed in 4% PFA in PB overnight, rinsed in PB, and cryoprotected
833 in 30% sucrose (in PB) for 48 h. Serial coronal sections (20 µm) were cut on a ThermoFisher NX70 cryostat,
834 thaw-mounted onto fluorescence-free SuperFrost$^+$ glass slides, and stored at -20 °C until processing. EdU
835 was visualized with Alexa 488-azide using the Click-iT labeling method (Life Technologies)[66].
836
837
838 **iTRAQ proteomics**
839 Single cortical hemispheres (n = 6/group, mixed and balanced for sex from independent pregnancies)
840 were obtained from E18.5 fetuses. Contralateral hemispheres were snap frozen for target validation by
841 real-time PCR and/or Western blotting. Proteins were extracted by homogenization in lysis buffer (pH
842 10.0) of triethylammonium bicarbonate (25 mM, Sigma), Na_2CO_3 (20 mM, Sigma) in the presence of pro-
843 tease inhibitors (Complete™, EDTA-free Protease Inhibitor Cocktail; Sigma). Protein concentrations were
844 determined by the bicinchoninic acid assay (ThermoFisher). After quantification, proteins were

845 precipitated in 6 volumes of ice-cold acetone. One hundred µg of proteins per sample were used for iso-
846 baric tagging for relative and absolute quantitation (iTRAQ) in an 8-plex layout per the manufacturer's
847 instructions (ABSciex). In brief, proteins were denatured, reduced, alkylated, trypsin digested (Promega),
848 individually labeled with appropriate iTRAQ tags, pooled, concentrated, re-suspended in 1.4 ml loading
849 buffer (10 mM KH2PO4, pH 3.0 in 25% acetonitrile) and sonicated.
850
851 Peptides were separated by cation exchange chromatography on a PolySulfoethyl A column (PolyLC) over
852 30 min with a KCl gradient increasing up to 0.5 M, with 0.5 ml fractions collected. Fifteen fractions across
853 the elution profile of similar peptide concentration were generated and concentrated (SpeedVac). Frac-
854 tions were re-suspended in 0.1% trifluoroacetic acid (TFA) and desalted on C18 spin columns (PepClean
855 C18, Thermo Scientific). Half of each fraction was then injected on an Acclaim PepMap 100 C18 trap and
856 an Acclaim PepMap RSLC C18 column (Thermo Scientific), using a nanoLC Ultra 2D plus loading pump and
857 nanoLC as-2 autosampler (Eksigent). The peptides were loaded onto the trap in a mixture of 98% water,
858 2% ACN and 0.05% TFA, washed for 20 min to waste before switching in line with the column, and were
859 then eluted with a gradient of increasing ACN, containing 0.1% formic acid (2-20% ACN in 90 min, 20-40%
860 in a further 30 min, followed by 98% ACN to clean the column before re-equilibration to 2% ACN). The
861 eluate was sprayed into a TripleTOF 5600 electrospray tandem mass spectrometer (ABSciex) and analyzed
862 in Information Dependent Acquisition (IDA) mode, performing 120 ms of MS followed by 80 ms MSMS
863 analyses on the 20 most intense peaks seen by MS, with the '*Adjust collision energy when using iTRAQ*
864 *reagent*' box ticked. The data files were processed by ProteinPilot 4.5 (Sciex) using the Paragon algorithm,
865 searching against the SwissProt database (March 2013 edition). The following settings were selected:
866 *sample type*: iTRAQ 8-plex (peptide labelled), *cysteine alkylation*: MMTS, *digestion*: trypsin, *instrument*:
867 TripleTOF 5600, *species*: mouse, *ID focus*: biological modifications and amino acid substitutions, and
868 *search effort*: thorough. Results were statistical evaluated in SPSS v. 21.
869
870
871 **Behavioral tests**
872 Anxiety-like behavior in first-generation offspring was assessed in the elevated plus maze on P75 (n = 6
873 males/group from independent pregnancies) as described[67-70]. Mice were placed in the center of a stand-
874 ard elevated plus maze apparatus (arms: 10 cm × 50 cm each) facing an open arm and allowed to explore
875 the maze for 5 min. The distance travelled (cm) and the number of arm entries (n) were determined.
876
877
878 **Statistical analysis and figure design**
879 The number of independent samples is indicated in either the individual figure panels or their associated
880 legends. Likewise, the number of animals is given where relevant. All values represent the means ± s.d. of
881 independent experiments. Biological variation among the samples was similar throughout. Statistical sig-
882 nificance was determined by either Student's t-test (for independent groups, two-tailed) or one-way and
883 two-way analysis of variance (ANOVA) followed by either Bonferroni's or Tukey's post-hoc correction (for
884 multiple groups). Statistical analysis was performed in Prism 8.0 (GraphPad). Statistical significance was
885 defined throughout unless stated in bulk as follows: *$p < 0.05$, **$p < 0.01$, ***$p < 0.001$, ****$p < 0.0001$.
886 Multi-panel images were assembled in CorelDraw 2022 using linear color, brightness, and contrast en-
887 hancement to increase visual clarity, if necessary.

References

1 Verkhratsky, A. & Butt, A. *Neuroglia: function and pathology*. (Elsevier, 2023).

2 Moore, B. W. A soluble protein characteristic of the nervous system. *Biochem Biophys Res Commun* **19**, 739-744, doi:10.1016/0006-291x(65)90320-7 (1965).

3 Leclerc, E., Sturchler, E. & Vetter, S. W. The S100B/RAGE Axis in Alzheimer's Disease. *Cardiovasc Psychiatry Neurol* **2010**, 539581, doi:10.1155/2010/539581 (2010).

4 Savchenko, V. L., McKanna, J. A., Nikonenko, I. R. & Skibo, G. G. Microglia and astrocytes in the adult rat brain: comparative immunocytochemical analysis demonstrates the efficacy of lipocortin 1 immunoreactivity. *Neuroscience* **96**, 195-203, doi:10.1016/s0306-4522(99)00538-2 (2000).

5 Xia, C., Braunstein, Z., Toomey, A. C., Zhong, J. & Rao, X. S100 Proteins As an Important Regulator of Macrophage Inflammation. *Front Immunol* **8**, 1908, doi:10.3389/fimmu.2017.01908 (2017).

6 Di Bella, D. J. *et al.* Molecular logic of cellular diversification in the mouse cerebral cortex. *Nature* **595**, 554-559, doi:10.1038/s41586-021-03670-5 (2021).

7 Hernandez-Ortega, K. *et al.* S100B actions on glial and neuronal cells in the developing brain: an overview. *Front Neurosci* **18**, 1425525, doi:10.3389/fnins.2024.1425525 (2024).

8 Xu, Q. *et al.* Profile and regulation of apolipoprotein E (ApoE) expression in the CNS in mice with targeting of green fluorescent protein gene to the ApoE locus. *J Neurosci* **26**, 4985-4994, doi:10.1523/JNEUROSCI.5476-05.2006 (2006).

9 Michalovicz, L. T. *et al.* Astrocyte-specific transcriptome analysis using the ALDH1L1 bacTRAP mouse reveals novel biomarkers of astrogliosis in response to neurotoxicity. *J Neurochem* **150**, 420-440, doi:10.1111/jnc.14800 (2019).

10 Dougherty, J. D., Schmidt, E. F., Nakajima, M. & Heintz, N. Analytical approaches to RNA profiling data for the identification of genes enriched in specific cells. *Nucleic Acids Res* **38**, 4218-4230, doi:10.1093/nar/gkq130 (2010).

11 Yamashita, N., Ilg, E. C., Schafer, B. W., Heizmann, C. W. & Kosaka, T. Distribution of a specific calcium-binding protein of the S100 protein family, S100A6 (calcyclin), in subpopulations of neurons and glial cells of the adult rat nervous system. *J Comp Neurol* **404**, 235-257 (1999).

12 Lesniak, W. & Filipek, A. S100A6 as a Constituent and Potential Marker of Adult and Cancer Stem Cells. *Stem Cell Rev Rep* **18**, 2699-2708, doi:10.1007/s12015-022-10403-2 (2022).

13 Graczyk, A. & Lesniak, W. S100A6 expression in keratinocytes and its impact on epidermal differentiation. *Int J Biochem Cell Biol* **57**, 135-141, doi:10.1016/j.biocel.2014.10.007 (2014).

14 Schneider, G. & Filipek, A. S100A6 binding protein and Siah-1 interacting protein (CacyBP/SIP): spotlight on properties and cellular function. *Amino Acids* **41**, 773-780, doi:10.1007/s00726-010-0498-2 (2011).

15 Filipek, A., Puzianowska, M., Cieslak, B. & Kuznicki, J. Calcyclin--Ca(2+)-binding protein homologous to glial S-100 beta is present in neurones. *Neuroreport* **4**, 383-386, doi:10.1097/00001756-199304000-00010 (1993).

16 Allaman, I., Belanger, M. & Magistretti, P. J. Astrocyte-neuron metabolic relationships: for better and for worse. *Trends Neurosci* **34**, 76-87, doi:10.1016/j.tins.2010.12.001 (2011).

17 Wasik, U., Kadziolka, B., Kilanczyk, E. & Filipek, A. Influence of S100A6 on CacyBP/SIP Phosphorylation and Elk-1 Transcriptional Activity in Neuroblastoma NB2a Cells. *J Cell Biochem* **117**, 126-131, doi:10.1002/jcb.25257 (2016).

18 Donato, R., Sorci, G. & Giambanco, I. S100A6 protein: functional roles. *Cell Mol Life Sci* **74**, 2749-2760, doi:10.1007/s00018-017-2526-9 (2017).

19 Karagoz, G. E., Acosta-Alvear, D. & Walter, P. The Unfolded Protein Response: Detecting and Responding to Fluctuations in the Protein-Folding Capacity of the Endoplasmic Reticulum. *Cold Spring Harb Perspect Biol* **11**, doi:10.1101/cshperspect.a033886 (2019).

20 Almanza, A. *et al.* Endoplasmic reticulum stress signalling - from basic mechanisms to clinical applications. *FEBS J* **286**, 241-278, doi:10.1111/febs.14608 (2019).

21 Marciniak, S. J. *et al.* CHOP induces death by promoting protein synthesis and oxidation in the stressed endoplasmic reticulum. *Genes Dev* **18**, 3066-3077, doi:10.1101/gad.1250704 (2004).

22 Trulsson, F. *et al.* Deubiquitinating enzymes and the proteasome regulate preferential sets of ubiquitin substrates. *Nat Commun* **13**, 2736, doi:10.1038/s41467-022-30376-7 (2022).

23 Malenczyk, K. *et al.* A TRPV1-to-secretagogin regulatory axis controls pancreatic beta-cell survival by modulating protein turnover. *EMBO J* **36**, 2107-2125, doi:10.15252/embj.201695347 (2017).

24 Tortoriello, G. *et al.* Miswiring the brain: Delta9-tetrahydrocannabinol disrupts cortical development by inducing an SCG10/stathmin-2 degradation pathway. *EMBO J* **33**, 668-685, doi:10.1002/embj.201386035 (2014).
25 Maruta, H., Greer, K. & Rosenbaum, J. L. The acetylation of alpha-tubulin and its relationship to the assembly and disassembly of microtubules. *J Cell Biol* **103**, 571-579, doi:10.1083/jcb.103.2.571 (1986).
26 Filipek, A., Jastrzebska, B., Nowotny, M. & Kuznicki, J. CacyBP/SIP, a calcyclin and Siah-1-interacting protein, binds EF-hand proteins of the S100 family. *J Biol Chem* **277**, 28848-28852, doi:10.1074/jbc.M203602200 (2002).
27 Borsini, A., Stangl, D., Jeffries, A. R., Pariante, C. M. & Thuret, S. The role of omega-3 fatty acids in preventing glucocorticoid-induced reduction in human hippocampal neurogenesis and increase in apoptosis. *Transl Psychiatry* **10**, 219, doi:10.1038/s41398-020-00908-0 (2020).
28 Borsini, A. *et al.* Omega-3 polyunsaturated fatty acids protect against inflammation through production of LOX and CYP450 lipid mediators: relevance for major depression and for human hippocampal neurogenesis. *Mol Psychiatry* **26**, 6773-6788, doi:10.1038/s41380-021-01160-8 (2021).
29 Yu, J. Z., Wang, J., Sheridan, S. D., Perlis, R. H. & Rasenick, M. M. N-3 polyunsaturated fatty acids promote astrocyte differentiation and neurotrophin production independent of cAMP in patient-derived neural stem cells. *Mol Psychiatry* **26**, 4605-4615, doi:10.1038/s41380-020-0786-5 (2021).
30 Laye, S., Nadjar, A., Joffre, C. & Bazinet, R. P. Anti-Inflammatory Effects of Omega-3 Fatty Acids in the Brain: Physiological Mechanisms and Relevance to Pharmacology. *Pharmacological reviews* **70**, 12-38, doi:10.1124/pr.117.014092 (2018).
31 Madore, C. *et al.* Essential omega-3 fatty acids tune microglial phagocytosis of synaptic elements in the mouse developing brain. *Nat Commun* **11**, 6133, doi:10.1038/s41467-020-19861-z (2020).
32 Chu, Q. *et al.* Regulation of the ER stress response by a mitochondrial microprotein. *Nat Commun* **10**, 4883, doi:10.1038/s41467-019-12816-z (2019).
33 Haggarty, P. Effect of placental function on fatty acid requirements during pregnancy. *Eur J Clin Nutr* **58**, 1559-1570, doi:10.1038/sj.ejcn.1602016 (2004).
34 Helland, I. B., Smith, L., Saarem, K., Saugstad, O. D. & Drevon, C. A. Maternal supplementation with very-long-chain n-3 fatty acids during pregnancy and lactation augments children's IQ at 4 years of age. *Pediatrics* **111**, e39-44, doi:10.1542/peds.111.1.e39 (2003).
35 Cinquina, V. *et al.* Life-long epigenetic programming of cortical architecture by maternal 'Western' diet during pregnancy. *Molecular psychiatry* **25**, 22-36, doi:10.1038/s41380-019-0580-4 (2020).
36 Zeng, C. *et al.* Evaluation of 5-ethynyl-2'-deoxyuridine staining as a sensitive and reliable method for studying cell proliferation in the adult nervous system. *Brain Res* **1319**, 21-32, doi:10.1016/j.brainres.2009.12.092 (2010).
37 Mulder, J. *et al.* Endocannabinoid signaling controls pyramidal cell specification and long-range axon patterning. *Proc Natl Acad Sci U S A* **105**, 8760-8765, doi:10.1073/pnas.0803545105 (2008).
38 Kepecs, A. & Fishell, G. Interneuron cell types are fit to function. *Nature* **505**, 318-326, doi:10.1038/nature12983 (2014).
39 Hipp, M. S., Kasturi, P. & Hartl, F. U. The proteostasis network and its decline in ageing. *Nat Rev Mol Cell Biol* **20**, 421-435, doi:10.1038/s41580-019-0101-y (2019).
40 Allen, N. J. & Eroglu, C. Cell Biology of Astrocyte-Synapse Interactions. *Neuron* **96**, 697-708, doi:https://doi.org/10.1016/j.neuron.2017.09.056 (2017).
41 Huang, E. J. & Reichardt, L. F. Neurotrophins: roles in neuronal development and function. *Annu Rev Neurosci* **24**, 677-736, doi:10.1146/annurev.neuro.24.1.677 (2001).
42 Goenaga, J., Araque, A., Kofuji, P. & Herrera Moro Chao, D. Calcium signaling in astrocytes and gliotransmitter release. *Front Synaptic Neurosci* **15**, 1138577, doi:10.3389/fnsyn.2023.1138577 (2023).
43 Donato, R. *et al.* Functions of S100 proteins. *Curr Mol Med* **13**, 24-57 (2013).
44 Santamaria-Kisiel, L., Rintala-Dempsey, Anne C. & Shaw, Gary S. Calcium-dependent and -independent interactions of the S100 protein family. *Biochemical Journal* **396**, 201-214, doi:10.1042/bj20060195 (2006).
45 Lesniak, W. & Filipek, A. S100A6 Protein-Expression and Function in Norm and Pathology. *Int J Mol Sci* **24**, doi:10.3390/ijms24021341 (2023).
46 Lesniak, W., Slomnicki, L. P. & Filipek, A. S100A6 - new facts and features. *Biochem Biophys Res Commun* **390**, 1087-1092, doi:10.1016/j.bbrc.2009.10.150 (2009).

47 Peng, Z. *et al.* EPA is More Effective than DHA to Improve Depression-Like Behavior, Glia Cell Dysfunction and Hippcampal Apoptosis Signaling in a Chronic Stress-Induced Rat Model of Depression. *Int J Mol Sci* **21**, doi:10.3390/ijms21051769 (2020).

48 Schiavi, S. *et al.* Perinatal supplementation with omega-3 fatty acids corrects the aberrant social and cognitive traits observed in a genetic model of autism based on FMR1 deletion in rats. *Nutr Neurosci* **25**, 898-911, doi:10.1080/1028415X.2020.1819107 (2022).

49 Cinquina, V., Keimpema, E., Pollak, D. D. & Harkany, T. Adverse effects of gestational omega-3 and omega-6 polyunsaturated fatty acid imbalance on the programming of fetal brain development. *J Neuroendocrinol* **35**, e13320, doi:10.1111/jne.13320 (2023).

50 Bae, S., Bessho, Y., Hojo, M. & Kageyama, R. The bHLH gene Hes6, an inhibitor of Hes1, promotes neuronal differentiation. *Development* **127**, 2933-2943, doi:10.1242/dev.127.13.2933 (2000).

51 Katakura, M. *et al.* Omega-3 polyunsaturated Fatty acids enhance neuronal differentiation in cultured rat neural stem cells. *Stem Cells Int* **2013**, 490476, doi:10.1155/2013/490476 (2013).

52 Calvigioni, D. *et al.* Functional Differentiation of Cholecystokinin-Containing Interneurons Destined for the Cerebral Cortex. *Cereb Cortex* **27**, 2453-2468, doi:10.1093/cercor/bhw094 (2017).

53 Tarhan, L. *et al.* Single Cell Portal: an interactive home for single-cell genomics data. *bioRxiv*, doi:10.1101/2023.07.13.548886 (2023).

54 Stuart, T. & Satija, R. Integrative single-cell analysis. *Nat Rev Genet* **20**, 257-272, doi:10.1038/s41576-019-0093-7 (2019).

55 Satija, R., Farrell, J. A., Gennert, D., Schier, A. F. & Regev, A. Spatial reconstruction of single-cell gene expression data. *Nat Biotechnol* **33**, 495-502, doi:10.1038/nbt.3192 (2015).

56 McInnes, L., Healy, J. & Melville, J. Umap: Uniform manifold approximation and projection for dimension reduction. *arXiv preprint arXiv:1802.03426* (2018).

57 Van der Maaten, L. & Hinton, G. Visualizing data using t-SNE. *Journal of machine learning research* **9** (2008).

58 Kobak, D. & Linderman, G. C. Initialization is critical for preserving global data structure in both t-SNE and UMAP. *Nature Biotechnology* **39**, 156-157, doi:10.1038/s41587-020-00809-z (2021).

59 Traag, V. A., Waltman, L. & van Eck, N. J. From Louvain to Leiden: guaranteeing well-connected communities. *Scientific Reports* **9**, 5233, doi:10.1038/s41598-019-41695-z (2019).

60 Ntranos, V., Yi, L., Melsted, P. & Pachter, L. A discriminative learning approach to differential expression analysis for single-cell RNA-seq. *Nature Methods* **16**, 163-166, doi:10.1038/s41592-018-0303-9 (2019).

61 Love, M. I., Huber, W. & Anders, S. Moderated estimation of fold change and dispersion for RNA-seq data with DESeq2. *Genome Biology* **15**, 550, doi:10.1186/s13059-014-0550-8 (2014).

62 Berghuis, P. *et al.* Hardwiring the brain: endocannabinoids shape neuronal connectivity. *Science* **316**, 1212-1216, doi:10.1126/science.1137406 (2007).

63 Onsurathum, S. *et al.* Proteomics detection of S100A6 in tumor tissue interstitial fluid and evaluation of its potential as a biomarker of cholangiocarcinoma. *Tumour Biol* **40**, 1010428318767195, doi:10.1177/1010428318767195 (2018).

64 Ho, J., Tumkaya, T., Aryal, S., Choi, H. & Claridge-Chang, A. Moving beyond P values: data analysis with estimation graphics. *Nature Methods* **16**, 565-566, doi:10.1038/s41592-019-0470-3 (2019).

65 Keimpema, E. *et al.* Differential subcellular recruitment of monoacylglycerol lipase generates spatial specificity of 2-arachidonoyl glycerol signaling during axonal pathfinding. *J Neurosci* **30**, 13992-14007, doi:10.1523/JNEUROSCI.2126-10.2010 (2010).

66 Ayoub, A. E. *et al.* Transcriptional programs in transient embryonic zones of the cerebral cortex defined by high-resolution mRNA sequencing. *Proc Natl Acad Sci U S A* **108**, 14950-14955, doi:10.1073/pnas.1112213108 (2011).

67 Archer, J. Tests for emotionality in rats and mice: a review. *Animal behaviour* **21**, 205-235 (1973).

68 Harkany, T. *et al.* N-Methyl-D-aspartate receptor antagonist MK-801 and radical scavengers protect cholinergic nucleus basalis neurons against beta-amyloid neurotoxicity. *Neurobiology of disease* **6**, 109-121, doi:10.1006/nbdi.1998.0230 (1999).

69 Harkany, T. *et al.* Beta-amyloid(Phe(SO3H)24)25-35 in rat nucleus basalis induces behavioral dysfunctions, impairs learning and memory and disrupts cortical cholinergic innervation. *Behavioural brain research* **90**, 133-145 (1998).

70 Walf, A. A. & Frye, C. A. The use of the elevated plus maze as an assay of anxiety-related behavior in rodents. *Nature protocols* **2**, 322-328, doi:10.1038/nprot.2007.44 (2007).

Legends to Figures

Figure 1. S100A6 and CaCyBp in the developing mouse brain. a. UMAP visualization of single-cell RNA-seq data from the somatosensory cortex during mouse brain development (from embryonic day (E) 10 to postnatal day (P) 4), and disaggregated by cell type. **b**-**d**. Identification of cell types (**b**), developmental stages (**c**), and astrocyte clusters (**d**) during corticogenesis. **e.** Single-cell RNA-seq-based developmental expression patterns for S100 proteins, calcyclin-binding protein (*Cacybp*), and *Siah1*a/b E3 ubiquitin ligases at the developmental time-points indicated. **f**. Violin plot showing the expression of *S100a6* in cell types. **g.** Cell type assignment for *S100a6* by UMAP at E18. **h.** Cell type assignment for *Cacybp* by UMAP at E18. **i**. Violin plot showing the expression of *Cacybp* per cell lineage.

Figure 2. Complementarity of S100A6 and calcyclin-binding protein expression in the cerebral cortex. a,d. *S100a6* mRNA expression overlapped with that of *S100b, Apoe, Aldh1l1*, and *Gfap* in both the fetal (E18.5; **a**) and neonatal (P4; **d**) mouse brain. Note the mutually exclusive expression of *S100a6* and *Rbfox3*, which encodes neuron-specific nuclear protein (NeuN). In contrast, *Cacybp* mRNA co-existed with that of *Rbfox3* but not *Gfap*, at both time points in development (**b,e**). **c,f**. Representative images and quantification of CaCyBp localization by immunohistochemistry in neurons of male fetal (E18.5; **c**) and neonatal (P4; **f**) mouse brains. Tissues were processed to simultaneously localize CaCyBp and either microtubule-associated protein 2 (MAP2; pan-neuronal marker) or calretinin (CR). Data are from n = 3 biological replicates. *Scale bars* = 12 μm

Figure 3. CaCyBp in human fetal brain and its complementarity with S100A6 *in vitro*

a. CaCyBp along the somatodendritic axis of cortical neurons in a human fetus at gestational week (GW) 27. The section was counterstained with hematoxylin/eosin (HE; *scale bar* = 8 μm). **b,c.** Comparison of *S100a6 vs*. *Cacybp* mRNA (**b**) and protein (**c**) levels in cultured neurons *vs*. astrocytes. mRNA expression was normalized to *Gapdh*, a housekeeping gene. Student's *t*-test; means ± s.d. from n = 3 independent experiments (mRNA neurons: n = 2 mice; ***p < 0.001; mRNA astrocytes: n = 3 mice; ***p < 0.001; protein S100A6: n = 3 mice; ****p < 0.0001; protein CaCyBp: n = 3 mice; ***p < 0.001).

Figure 4. Astrocyte-derived S100A6 limits neuritogenesis. a. ELISA of S100A6 in culture media upon glutamate (100 μM) exposure for 24 h. (n = 3 biological replicates; mixed for sex; *p = 0.044 [0 h] *vs*. [6 h]; **p = 0.001 [6 h] *vs*. [24 h]; ***p < 0.0001 [0 h] *vs*. [24 h], one-way ANOVA followed by Tukey's multiple comparisons). **b**. Cultured mouse astrocytes were stimulated with glutamate (100 μM) *vs*. control. Data were normalized to cell density prior to glutamate exposure on day 1 *in vitro* (DIV, n = 8 biological replicates, mixed for sex). **c.** Neuro-2a cells were treated with His-tagged recombinant S100A6 (1 μg/μl) for 1 h and double-labelled for F-actin (phalloidin; *green*) and anti-S100A6 (*magenta*). DAPI, a nuclear counterstain, was color-coded in white. *Scale bar* = 8 μm. **d**. S100A6 was identified in Neuro-2a cells 1 h after exposure by liquid-chromatography coupled with tandem mass spectrometry (2 unique peptides, sequence coverage 21.1 %). S100A6 was not present in any of the control samples. Detected mass-to-charge ratio (m/z), charge state (z), error in parts per million (ppm), unique peptide sequences, and sequence

coverage were defined. **e.** Morphometric analysis of cortical neurons exposed to recombinant His-tagged S100A6 (1 μg/μl) for 4 DIV. Data were normalized to neurite length prior to S100A6 exposure on 1 DIV. S100A6 reduced neurite complexity. '*Body cluster area*' refers to the surface occupancy of neurons after 4 DIV, and was taken as a measure of cell survival (n = 3 biological replicates; mixed for sex; $^{**}p$ = 0.003; Student's *t*-test). **f.** CaCyBp in cortical neurons was reduced after recombinant S100A6 (1 μg/μl) exposure for 4 DIV (n = 3 biological replicates; mixed for sex; $^{**}p$ = 0.005; Student's *t*-test). Data were normalized to GAPDH. **g**. Neuritogenesis of cortical neurons (P0) was reduced 15 DIV after exposure to shRNA for *CaCyBp* (sh*CaCyBp*). Primary neurite length (μm) was normalized to mock-transfected controls (n = 23-27 cells; mixed for sex; $^{***}p$ = 0.0004 *vs*. mock-transfected control; Student's *t*-test; *scale bar* = 12 μm). **h**. mRNA levels for *Tubb3* ($^{*}p$ = 0.045 [sh*Cacybp*] *vs*. [control]; $^{*}p$ = 0.048 [His-S100A6] *vs*. [control]; $^{**}p$ = 0.002 [sh*Cacybp*+his-S100A6] *vs*. [control), and *Actb* ($^{*}p$ = 0.027 [sh*Cacybp*] *vs*. [control]; $^{**}p$ = 0.008 [His-S100A6] *vs*. [control]; $^{**}p$ = 0.005 [sh*Cacybp*+his-S100A6] *vs*. [control]) in cortical neurons (P0) after transfection with sh*Cacybp* followed by treatment with recombinant His-S100A6. Data were normalized to *Gapdh*, a housekeeping standard (n = 5-10 biological replicates; mixed for sex; Student's *t*-test). **i**. Neurite numbers after combined treatment with sh*Cacybp* followed by His-S100A6 protein exposure. Number of neurons were normalized to mock-transfected control (n = 5-8 cells; mixed for sex; one-way ANOVA followed by Tukey's multiple comparisons). **j**. Neuritogenesis was reduced 24 h after dual manipulation (sh*Cacybp* and His-S100A6). Primary neurite and total neurite length (μm) were normalized to mock-transfected controls and expressed as percentage (n = 3-6 cells; mixed for sex; *primary neurite length:* $^{***}p$ = 0.0003 [sh*Cacybp*] *vs*. [control]; $^{**}p$ = 0.003 [His-S100A6] *vs*. [control]; $^{**}p$ = 0.002 [sh*Cacybp*+his-S100A6] *vs*. [control]; *neurite length*: $^{*}p$ = 0.0102 [sh*Cacybp*] *vs*. [control]; $^{**}p$ = 0.004 [His-S100A6] *vs*. [control]; $^{*}p$ = 0.023 [sh*Cacybp*+his-S100A6] *vs*. [control]; one-way ANOVA followed by Tukey's multiple comparison; *scale bar* = 12 μm). **k**. Schema of the putative molecular pathway.

Figure 5. CaCyBp modulates protein turnover in neurons. a. After subcellular fractionation, CaCyBp was detected in both cytosol and endoplasmatic reticulum (ER) fractions by Western blotting. Cofilin and calnexin in the cytosol *vs*. ER fraction were used to showcase subcellular enrichment. **b.** CaCyBp accumulated around the endoplasmic reticulum (*white arrowheads*) in hippocampal neurons. *Scale bars* = 500 nm (12,500x) and 1 μm (6,200x). **c.** Western analysis of total protein content in cortical neurons after sh*Cacybp* exposure (n = 4 male mice; $^{**}p$ = 0.005 *vs*. mock-transfected controls; Student's *t*-test). **d.** mRNA levels for *Grp78* ($^{**}p$ = 0.001), *Atf4*, *Atf6a* ($^{**}p$ = 0.008), *Chop*, *Xbp1u* ($^{***}p$ < 0.001) and *Xbp1s* ($^{**}p$ = 0.002) in cortical neurons after sh*Cacybp* exposure. Data were normalized to *Gapdh*, a housekeeping standard (n = 6 biological replicates; mixed for sex; Student's *t*-test). **e**. Western blot detection of ubiquitin-specific protease 7 (USP7; 128 kDa; n = 3 biological replicates; mixed for sex; Student's *t*-test) and ubiquitin-specific protease 9X (USP9X; 270k Da; $^{**}p$ = 0.0076 *vs*. mock-transfected controls, n = 3 biological replicates; mixed for sex; Student's *t*-test) in cortical neurons exposed to sh*Cacybp*. Data were normalized to GAPDH. **f.** Western blot detection of acetylated tubulin (50kDa) in cortical neurons exposed to sh*Cacybp* ($^{****}p$ < 0.0001 *vs*. mock-transfected control; n = 3 biological replicates; mixed for sex, Student's *t*-test). Data were normalized to GAPDH. **g.** Neuro-2a cells were exposed to shRNA for *Cacybp*, followed by exposure to His-tagged recombinant S100A6 (1 μg/μl) for 1 h. Subsequently, cells were double-labelled for F-actin (phalloidin; *green*) and anti-S100A6 (*magenta*). DAPI, a nuclear counterstain, was color-coded in white. *Scale bar* = 8 μm. **h.** ELISA of S100A6 in the cytosol and ER fraction of Neuro-2a cells

upon the manipulations indicated (n = 3 biological replicates; mixed for sex; *p = 0.021 [cytosol] *vs.* [ER] after S100A6; *p = 0.022 [cytosol] *vs*. [ER] after sh*Cacybp*+S100A6 exposure; **p = 0.004 [ER] *vs.* [ER] after sh*Cacybp*+S100A6 exposure; two-way ANOVA followed by Bonferroni's multiple comparisons).

Figure 6. S100A6 signaling is modulated by eicosapentaenoic acid. a. Neuritogenesis in cortical neurons (prepared at E18.5) treated with EPA as indicated at either 1 μM or 5 μM concentration, and monitored by dynamic live-cell imaging for 7 days *in vitro* (DIV). Data were normalized to neurite length prior to drug exposure on 1 DIV. Neurite outgrowth was determined by using a manual overlay of each neuron. Data are from n = 7 independent experiments (*neurite length*: $^{/}p$ = 0.038 [1 μM] *vs.* [control]; $^{/}p$ = 0.021 [1 μM] *vs.* [control]; **p = 0.006 [5 μM] *vs.* [control]; ***p = 0.0005 [5 μM] *vs.* [control]; ****p < 0.0001 [5 μM] *vs.* [control]; *neurite branches*: $^{/}p$ = 0.032 [1 μM] *vs.* [control]; $^{/}p$ = 0.014 [1 μM] *vs.* [control]; $^{/}p$ = 0.022 [1 μM] *vs.* [control]; **p = 0.007 [5 μM] *vs.* [control]; ***p = 0.0004 [5 μM] *vs.* [contro]l; ****p < 0.001 [5 μM] *vs.* [control]; two-way ANOVA followed by Tukey's multiple comparisons. **b**. Cultured mouse astrocytes were stimulated with EPA (30 μM) *vs*. control. Data were normalized to cell density prior to EPA exposure on 1 DIV. **c**. ELISA of S100A6 in culture media upon EPA (30 μM) exposure for 24 h (n = 3 biological replicates; mixed for sex; ****p < 0.0001 [0 h] *vs*. [24 h], ***p = 0.0004 [6 h] *vs*. [24 h]; one-way ANOVA followed by Tukey's multiple comparisons). **d**. mRNA levels for *Cacybp* (*p = 0.021; n = 3 biological replicates; mixed for sex; Student's t-test) in cortical neurons after exposure to a medium pre-conditioned for 24 h. **e.** mRNA levels for *Grp78* (*p = 0.024), *Atf4* (**p = 0.006), *Atf6a* (****p < 0.0001), *Chop*, *Xbp1u* (p = 0.061) and *Xbp1s* in E18.5 cortical neurons after exposure to astrocyte-conditioned medium for 24 h (n = 3 biological replicates; mixed for sex; Student's t-test). Data were expressed as means ± s.d. throughout.

Figure 7. S100A6 availability modulates neuronal differentiation. a. Schema of co-culture experiments. **b**. Western blot detection of S100A6 (10kDa) in the cytosol of astrocytes exposed to either scrambled or targeting siRNA for 96 h, and subsequently to EPA (30 μM) for another 6 h. Representative blots are shown. Numbers were used in subsequent panels for visual simplicity. **c**. ELISA of S100A6 in culture media upon siRNA exposure for 96 h followed by EPA (30 μM) exposure for 24 h. (n = 3-4 biological replicates; mixed for sex; *p = 0.039 [control] *vs.* [EPA + siRNA]; **p = 0.008 [EPA] *vs.* [EPA + siRNA]; one-way ANOVA followed by Tukey's multiple comparisons). **c_1**. S100A6 detected in astrocytes cytosol after the treatment as in (c). Data were from n = 3 biological replicates; mixed for sex; ****p < 0.0001 [siRNA] *vs.* [control]; ****p < 0.0001 [scrambled] *vs*. [siRNA]; ***p = 0.001 [EPA] *vs.* [control]; ***p = 0.0003 [siRNA] *vs.* [EPA]; **p = 0.0011 [scrambled] *vs.* [EPA]; ***p = 0.0003 [EPA] *vs.* [EPA + siRNA]; *p = 0.0106 [EPA] *vs.* [EPA + scrambled]; one-way ANOVA followed by Tukey's multiple comparisons). **d**. Representative imagines of cortical neurons exposed to the media indicated for 24 h. EPA (30 μM) directly applied onto neurons was included on the right. Neurons double-labelled for F-actin (phalloidin; *magenta*) and MAP2 (*green*) were shown with their lead neurites indicated by dashed lines, and their growth cones by solid *arrowheads*. *Scale bars* = 12 μm (*top*), 5 μm (*bottom*). DAPI, a nuclear counterstain, was color-coded in white. **e**. Primary neurite length after experimental manipulations was normalized to those in control (n = 5-9 cells; mixed for sex; *p = 0.042 [cond. siRNA] *vs.* [control]; **p = 0.001 [cond. EPA] *vs.* [control]; ****p < 0.0001 [EPA] *vs.* [control]; ***p = 0.0004 [cond. EPA] *vs.* [cond. siRNA]; **p = 0.001 [cond. EPA] *vs.* [EPA]; ***p

= 0.0006 [cond. EPA] *vs.* [cond. siRNA + EPA]; ****p < 0.0001 [cond. siRNA + EPA] *vs.* [EPA]; one-way ANOVA followed by Tukey's multiple comparisons). **f**. Neuritogenesis after the above manipulations and monitored by dynamic live-cell imaging for 24 h. Data were normalized to neurite length prior to treatment exposure and expressed in percentage. Neurite outgrowth was determined by using a manual overlay. Data were from n = 7-8 independent experiments (*neurite length*: **p = 0.001 [cond. EPA] *vs.* [control]; ****p < 0.0001 [EPA] *vs.* [control]; ***p = 0.0005 [cond. EPA] *vs.* [cond. siRNA + EPA]; **p = 0.008 [cond. EPA] *vs.* [EPA];
neurite branches: ***p = 0.0001 [cond. siRNA] *vs.* [control]; **p = 0.007 [cond. EPA] *vs.* [control]; ****p < 0.0001 [EPA] *vs.* [control]; ****p < 0.0001 [cond. siRNA] *vs.* [cond. EPA]; *p = 0.033 [cond. siRNA] *vs.* [cond. siRNA + EPA]; ****p < 0.0001 [cond. siRNA] *vs.* [EPA]; *p = 0.025 [cond. EPA] *vs.* [cond. siRNA + EPA]; ****p < 0.0001 [cond. EPA] *vs.* [EPA]; ****p < 0.0001 [cond. siRNA + RNA] *vs.* [EPA]; one-way ANOVA followed by Tukey's multiple comparisons). Data were expressed as means ± s.d. throughout.

Figure 8. Transgenerational modulation of S100A6 signaling. a. Representative images (*left*) and quantification (*right*) of EdU^+ neurons in cortical layers of male embryos at E18.5. Cell counting was performed in binned layers (numbered consecutively from 1 to 10) on equal tissue surfaces, and expressed as absolute numbers. (*Layer* 2: *p = 0.016; *Layer 5*: **p = 0.003; *layer 6*: *p = 0.026; *layer* 9: *p = 0.028). *Scale bars* = 20 μm. *Abbreviations*: cp, cortical plate; MZ, marginal zone; SVZ, subventricular zone. **b.** Classification of significantly altered proteins in mixed sex embryos through primary function assignment by gene ontology. Dams were exposed to a hypercaloric diet enriched in ω-3 fatty acids (**Supplementary Table 1**). **c.** Topmost modified proteins targets, with CaCyBp significantly down-regulated after gestation experimental diet exposure. In contrast, S100A6 was up-regulated. Only proteins contributing to the morphological differentiation of neurons were included (*see also* **Supplementary Table 2**). **d.** Western analysis of S100A6 and CaCyBp protein levels (n = 3 male mice/group; ****p < 0.0001, **p = 0.003 *vs.* standard diet; Student's *t*-test) in the cerebri of male embryos on E18.5. Data were normalized to GAPDH. **e.** Total protein content of cerebral tissues from male embryos at E18.5 (n = 3 male mice/group; **p = 0.001 *vs.* standard diet; Student's *t*-test). **f.** Western analysis of acetylated tubulin (50 kDa) in the cortices of male embryos at E18.5 in control and after exposure to an experimental diet (n= 3 male mice/group; **p = 0.002 vs. standard diet; Student's *t*-test). Data were normalized to GAPDH. **g**. Elevated plus maze test results expressed as 'distance travelled' (cm) and 'number of arm entries' (n) from n = 5-6 adult male mice/group (*p = 0.023 *vs.* standard diet; Student's *t*-test).

Legends to Supplementary Figures

Supplementary Figure 1. S100A6 and CaCyBp in the developing mouse brain. a. UMAP plot showing the distribution of *S100a6* expression on postnatal day 4 (P4). **b.** UMAP plot showing the distribution of *S100a6*$^+$/*S100b*$^+$, *S100a6*$^+$/*Apoa*$^+$, and *S100a6*$^+$/*Aldh1l1*$^+$ astrocytes. **c**. *S100a6* expression (mRNA) during fetal brain development, quantified by qPCR and normalized to *Gapdh* as a housekeeping standard from *n* = 4-7 male mice/time point (***p* = 0.003 for E14.5 *vs*. P4, one-way ANOVA followed by Tukey's multiple comparisons). **d**. Western analysis of S100A6 protein levels during pre- and neonatal life. Data were normalized to the total protein content of the samples (*n* = 3 male mice/time point; **p* = 0.017 for E18.5 *vs*. P4, Student's *t*-test). **e**. Schematic representation of S100A6 domains (residues 1-89). An S100A6 monomer consists of two EF-hand domains, which are the structural motifs for Ca^{2+} binding. **f**. Schematic representation of CaCaCyp (residues 1-229), including effector protein binding sites. **g.** UMAP plot of the distribution of *Cacybp* expression on P4. **h**. *Cacybp* mRNA expression during fetal brain development, normalized to *Gapdh* (***p* = 0.009 for E14.5 *vs*. P4, one-way ANOVA followed by Tukey's multiple comparisons). **i**. CaCyBp protein levels in the mouse cerebral cortex at the ages indicated (*n* = 3 male mice/time point, **p* = 0.0497 for E18.5 *vs*. P4, Student's *t*-test). Data were expressed as means ± s.d. throughout.

Supplementary Figure 2. **Localization of S100a6 in cortical astrocytes.** Overlapping expression of *S100a6* with *S100b* (**a**), *Apoe* (**b**), *Aldh1l1* (**c**), and *Gfap* (**d**) transcripts in the somatosensory cortex at fetal (E18.5) and neonatal (P4) ages. Note the mutually exclusive pattern between mRNA expression for *S100a6* and *Rbfox3*, the latter encoding neuron-specific nuclear protein (NeuN). Figures are representative from *n* = 3 male mice/time point. Dashed rectangles denote the location of high-resolution images in Figure 2. *Scale bars* = 10 μm.

Supplementary Figure 3. **CaCyBp localization in cortical neurons. a,b**. Overlap between the expression of *Cacybp* with *Rbfox3* (NeuN) transcripts in fetal (E18.5; **a**) and neonatal (P4; **b**) mouse cortices (representative images from *n* = 3 male mice/time point; *scale bars* = 10 μm (a,b)). **c,d.** Representative images of CaCyBp localization by immunohistochemistry in the somatosensory cortex of fetal (E18.5; **c**) and neonatal (P4, **d**) mice co-stained for either microtubule-associated protein 2 (MAP2) or calretinin (CR; representative images from *n* = 3 male mice/time point; *scale bars* = 50 μm (**c,d**)). Dashed boxes in panels (**a-d**) denote the localization of insets in Figure 2c,f. **e**. Neuronal localization of CaCyBp in the adult mouse cerebral cortex (P120) by co-labelling for NeuN (representative from *n* = 3 male mice/time point; *scale bar* = 60 μm). Open rectangle ('1') denote the localization of insets (*scale bar* = 10 μm). **f.** CaCyBp localization to the somatodendritic axis of cortical neuron-like cells in the adult human brain (60 years; male subject; *scale bar* = 250 μm). **g**. mRNA levels for *Map2* (*****p* < 0.0001), *Tubb3* (***p* = 0.003), *S100b* (***p* = 0.007), and *Aldh1l1* (***p* = 0.009; all with Student's *t*-test) in cultured neurons *vs*. astrocytes harvested from *n* = 4-5 mice (mixed for sex). mRNA expression was normalized to *Gapdh*, a housekeeping gene. *Abbreviations*: I-IV, cortical layers 1-4; astroc., astrocytes; cp, cortical plate; MZ, marginal zone; SVZ, subventricular zone.

Supplementary Figure 4. **Intracellular S100A6 variations and validation of knock-down experiments**. **a**. MTT assay showed the lack of astrocyte cell death upon glutamate treatment (100 μM; at 24 h). Floating plots show the overall weighted mean difference for all experiment (*n* = 8 biological replicates; mixed for sex; *see Methods*). Solid circles represent the point estimate of the mean difference, with vertical lines indicating 95% confidence intervals. The shaded curve represents the resampled distribution of the effect size. **b**. S100A6 in the cytosol of astrocytes (*left*) and cell-free culture medium (*right)* after treatment with glutamate (100 μM) for 24 h. Quantitative data are from quadruple experiments; cytosol: **p* = 0.021 [2 h] *vs*. [0 h]; **p* = 0.021 [6 h] *vs*. [0 h]; medium: ****p* < 0.001 [1 h] *vs*. [0 h]; *****p* < 0.0001 [2,4,6 h] *vs*. [0 h]; one-way ANOVA followed by Bonferroni's multiple comparisons. **c**. Western analysis of CaCyBp and S100A6 in Neuro-2a cells. **d**. Two unique S100A6 peptide fragments were identified by means of LC-MS/MS after exposure of Neuro-2a cells to recombinant S100A6 protein (1 μg/ml) in Neuro-2a for 24 h. **e**. Recombinant S100A6 protein was analyzed under identical conditions with data compared. Detected mass-to-charge ratio (m/z), charge state (z), error in parts per million (ppm), unique peptide sequences, and sequence coverage were provided. **f**. Representative images of cortical neurons at 15 DIV after being transfected with either scrambled shRNA (control) or shRNA against CaCyBp (sh*Cacybp*). Constructs were tagged with green fluorescence protein to validate expression efficacy (*bottom row*). *Scale bars* = 200 μm. **g**. mRNA levels of *Cacybp* in cortical neurons transfected with sh*Cacybp* for 15 days. mRNA levels were quantified by qPCR and normalized to *Gapdh*. *****p* < 0.0001, Student's *t*-test. Data are from *n* = 9 independent experiments. **h.** Western analysis of CaCyBp protein content from the same experiments. ****p* = 0.0002 (one-way ANOVA following by Bonferroni multiple caparisons). Data are from *n* = 6 independent experiments. Data were expressed as means ± s.d. throughout.

Supplementary Figure 5. **Recombinant S100A6 affects the UPR machinery. a**. Electron microscopy images of negative control, and CaCyBp localization in the vicinity of the endoplasmic reticulum (*black arrowheads*) of neurons in the dentate gyrus of the adult mouse brain. *Scale bars* = 500 nm (12,500x) and 1 μm (6,200x). *Abbreviations*: CF, cytosol fraction; ER, endoplasmic reticulum; N, nuclei. **b.** Total protein content after exposure to recombinant S100A6 (1 μg/μl) for 24 h *in vitro* (*n* = 4 biological replicates; mixed for sex; **p* = 0.04 *vs.* control, Student's *t*-test). **c**. Western blot detection of acetylated tubulin (50kDa) in cortical neurons after treatment with recombinant S100A6 for 24 h (from *n = 3* biological replicates; mixed for sex; ***p* = 0.001 *vs.* control, Student's *t*-test). Data were normalized to GAPDH. **d**. Western blot detection of ubiquitin-specific protease 7 (USP7; 128 kDa; *n = 3* biological replicates; mixed for sex; ***p* = 0.001 *vs.* control, Student's *t*-test) and ubiquitin-specific protease 9X (USP9X; 270 kDa; *n = 3* biological replicates; mixed for sex) in cortical neurons exposed to recombinant S100A6. Data were normalized to GAPDH. **e**. mRNA levels for *Cacybp* (*****p* < 0.0001 *vs.* control; *n = 6* biological replicates; mixed for sex) in cortical neurons (E18.5) after S100A6 exposure (1 μg/μl) for 24 h. **f.** *Grp78* (****p* < 0.001), *Atf4*, *Atf6a* (***p* = 0.002), *Chop* (****p* < 0.001), *Xbp1u* (****p* < 0.001), *Xbp1s* (***p* = 0.0013) mRNA levels in cortical neurons after exposure to recombinant S100A6 for 24 h. Data were normalized to *Gapdh*. Data were expressed as means ± s.d.; from *n* = 6 independent experiments.

Supplementary Figure 6. **Recombinant S100A4 lacks an effect on either neuronal growth or the UPR machinery. a.** UMAP plot of the distribution of *S100A4* expression on E18. **b**. Neuritogenesis of cortical

neurons (harvested at P0) was not reduced after exposure to recombinant S100A4 protein (1 μg/μl) for 24 h (*Scale bar* = 12 μm). Primary neurite length (μm) was normalized to mock-transfected controls and expressed as percentage (*n* = 16-21 cells/treatment; mixed for sex). **c**. mRNA levels for *Cacybp, Grp78, Atf4, Chop, Xbp1u*, and *Xbp1s* in cortical neurons after exposure to recombinant S100A4 (1 μg/μl) for 24 h. Data were normalized to *Gapdh*. Data were expressed as means ± s.d.; from duplicate experiments.

Supplementary Figure 7. **Eicosapentaenoic acid affects astrocyte viability and S100A6 release. a**. MTT assay showed neuronal viability upon EPA treatment (1 μM and 5 μM; at 7 DIV). Floating plots show the overall weighted mean difference for all experiment (*n* = 8 biological replicates; mixed for sex; *see Methods*). Solid circles represent the point estimate of the mean difference, with vertical lines indicating 95% confidence intervals. The shaded curve represents the resampled distribution of the effect size. **b**. Cultured astrocytes were stimulated with either EPA 5 μM (**a**) or 10 μM (**a**$_1$) *vs*. control. Data were normalized to cell density prior to EPA exposure on day 1 (*n* = 6 independent experiments; mixed for sex). **c**. Astrocyte viability (MTT assay) after EPA stimulation (5 μM, 10 μM, or 30 μM) for 24 h. Floating plots show the overall weighted mean difference for all experiment (*n* = 6 independent experiment; mixed for sex). Circles represent the point estimate of the mean difference, with vertical lines indicating 95% confidence intervals. The shaded curve represents the resampled distribution of the effect size. **d**. ELISA of S100A6 in culture media upon either 5 μM or 10 μM EPA stimulation for 24 h (*n* = 3 biological replicates; mixed for sex; **p* = 0.015 [0 h] *vs*. [24 h] (EPA 5 μM), **p* = 0.035 [0 h] *vs*. [6 h] (EPA 10 μM); ****p* = 0.035 [0 h] *vs*. [24 h] (EPA 10 μM); ***p* = 0.002 [6 h] *vs*. [24 h] (EPA 10 μM); one-way ANOVA followed by Tukey's multiple comparisons). **e**. Schema of co-culture experiments.

Supplementary Figure 8. **Conditioned astrocyte medium affects neurite outgrowth. a**. Primary neurite length was unchanged 24 h after exposure either to neuronal media (Neurobasal/B27) or conditioned astrocyte medium. Primary neurite length was normalized to neurons in Neurobasal/B27, and expressed as percentages (*n* = 7-8 cells; mixed for sex). **b.** Neuritogenesis in cortical neurons (E18.5) grown in Neurobasal/B27 or medium pre-conditioned by astrocytes, and monitored by dynamic live-cell imaging (IncuCyte) for 24 h. Data were normalized to neurite length prior to exposure to astrocyte-conditioned media. Neurite outgrowth was determined by using a manual overlay of each neuron (data from *n* = 8 independent experiments. Statistical evaluation: *neurite length*: ***p* = 0.014 *vs.* neuronal media; *****p* < 0.0001 *vs.* neuronal media; *neurite branches*: ****p* = 0.0001 *vs.* neuronal media; *****p* < 0.0001 *vs.* neuronal media. **c**. mRNA levels for *Cacybp* in cortical neurons after exposure to conditioned medium from astrocytes for 24 h. Data were normalized to *Gapdh*. Data are from *n* = 3-5 independent experiments; **p* = 0.02 [cond. siRNA] *vs.* [control]; *****p* < 0.0001 [cond. EPA] *vs.* [control]; **p* = 0.0224 [cond. EPA] *vs* [cond. siRNA+EPA]. Data were expressed as means ± s.d. followed by multiple comparisons after one-way ANOVA.

Supplementary Figure 9. **Dysregulation of corticogenesis in embryos exposed to an experimental diet rich in ω-3 polyunsaturated fatty acids. a.** Schema of diet administration to C57Bl6/J dams. Administration of the experimental diet commenced 8 weeks before gestation, and continued throughout gestation,

and lactation. **b**. Quantification of EdU^+ cell numbers in cortical layers of male embryos at E18.5. Cell counting was performed on equal cortical tissue surfaces, and expressed as absolute numbers (*n* = 2 male mice/group). **c**. Immunohistochemical detection of GAP43, MAP2, and NeuN in the somatosensory cortex of fetal mice (E18.5) after standard (*upper*) *vs*. experimental diet (*bottom*) exposure (*n* = 3 male mice/group from independent pregnancies). **d**. Immunoreactivity corresponding to GAP43 and MAP2 in E18.5 mouse cortices after experimental diet exposure was reduced by ~65% and ~45%, respectively, as compared to a standard diet. Neither $DAPI^+$ cell numbers nor NeuN immunoreactivity changed (*n* = 3 male mice/group; *$p = 0.018$ *vs.* standard diet; ****$p < 0.0001$ *vs.* standard diet; Student's *t*-test). *Scale bar* = 50 μm (d). *Abbreviations*: cp, cortical plate; IZ, intermediate zone; MZ, marginal zone; PND, postnatal day; VZ/SVZ, ventricular zone/subventricular zone.

Legends to Supplementary Tables

Supplementary Table 1. Composition of experimental and control diets used in this study. Deviation in composition between batches of the diets did not exceed 1% per constituent. Data are from Special Diet Services (UK) and were produced by mass-spectrometry as part of the standard quality control process.

Supplementary Table 2. Proteins with levels significantly modified in the cortices of male mouse fetuses after gestational exposure to an experimental diet. Comparative analysis of $n = 3$ (ω-3 fatty acid/vehicle) with data expressed as percentage deviation from the mean control value. Hits with statistically significant differences only were included, as evaluated by the Wilcoxon signed-rank test. Colored backgrounds identify data clusters with positive/negative differences from vehicle-treated controls.

Supplementary Table 3. Antibodies used for immunofluorescence histochemistry and Western blotting. Application-specific dilutions, hosts, and vendors of the antibodies included in this study were stated.

Supplementary Table 4. Primer sequences used in this study. qPCR reactions were performed with primer pairs amplifying short fragments for each gene. Primer pairs were custom designed to efficiently anneal to homologous nucleotide sequences from mouse.

Cinquina *et al*. - Figure 1 (revised manuscript)

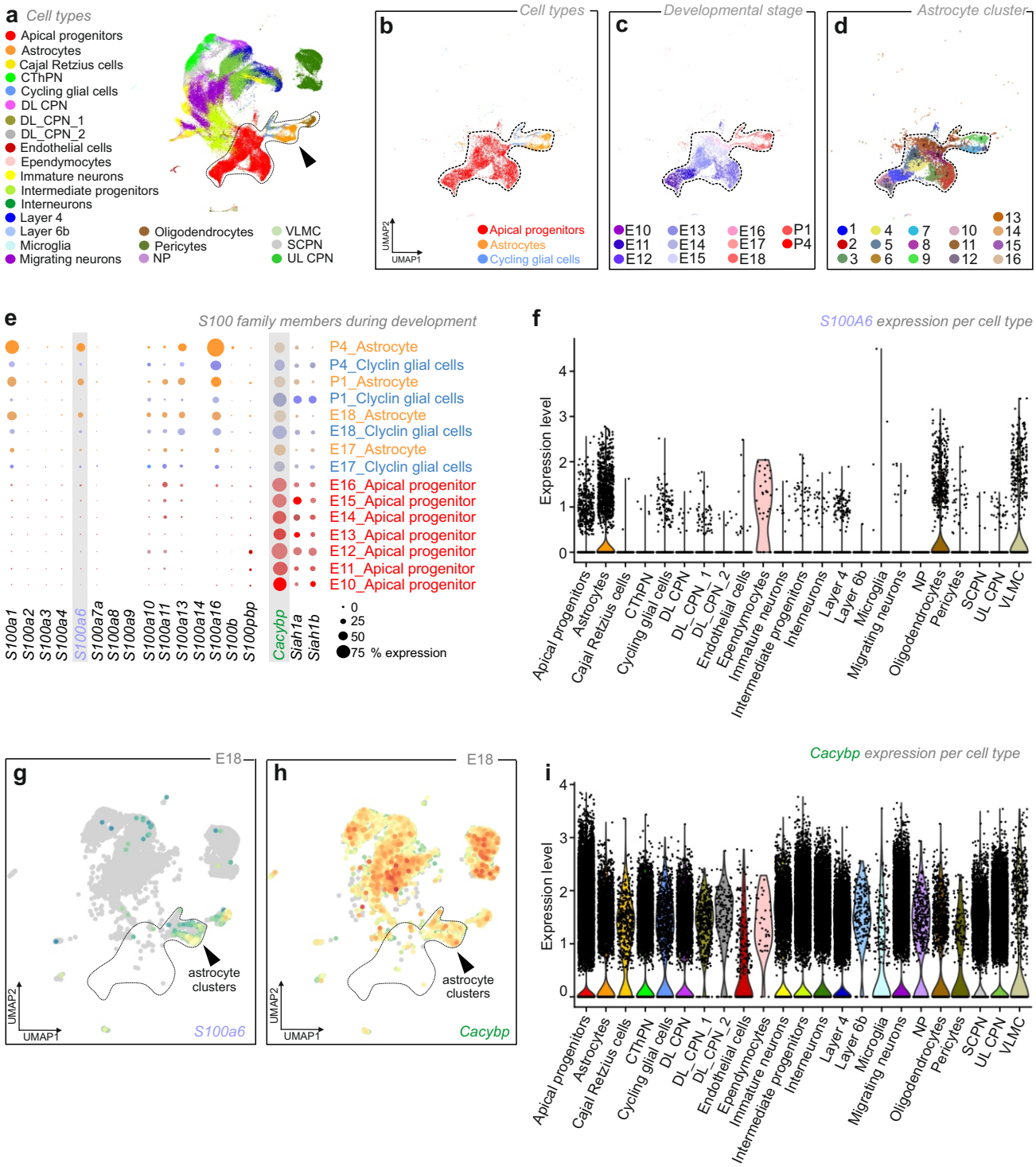

Cinquina *et al*. - Figure 2 (revised manuscript)

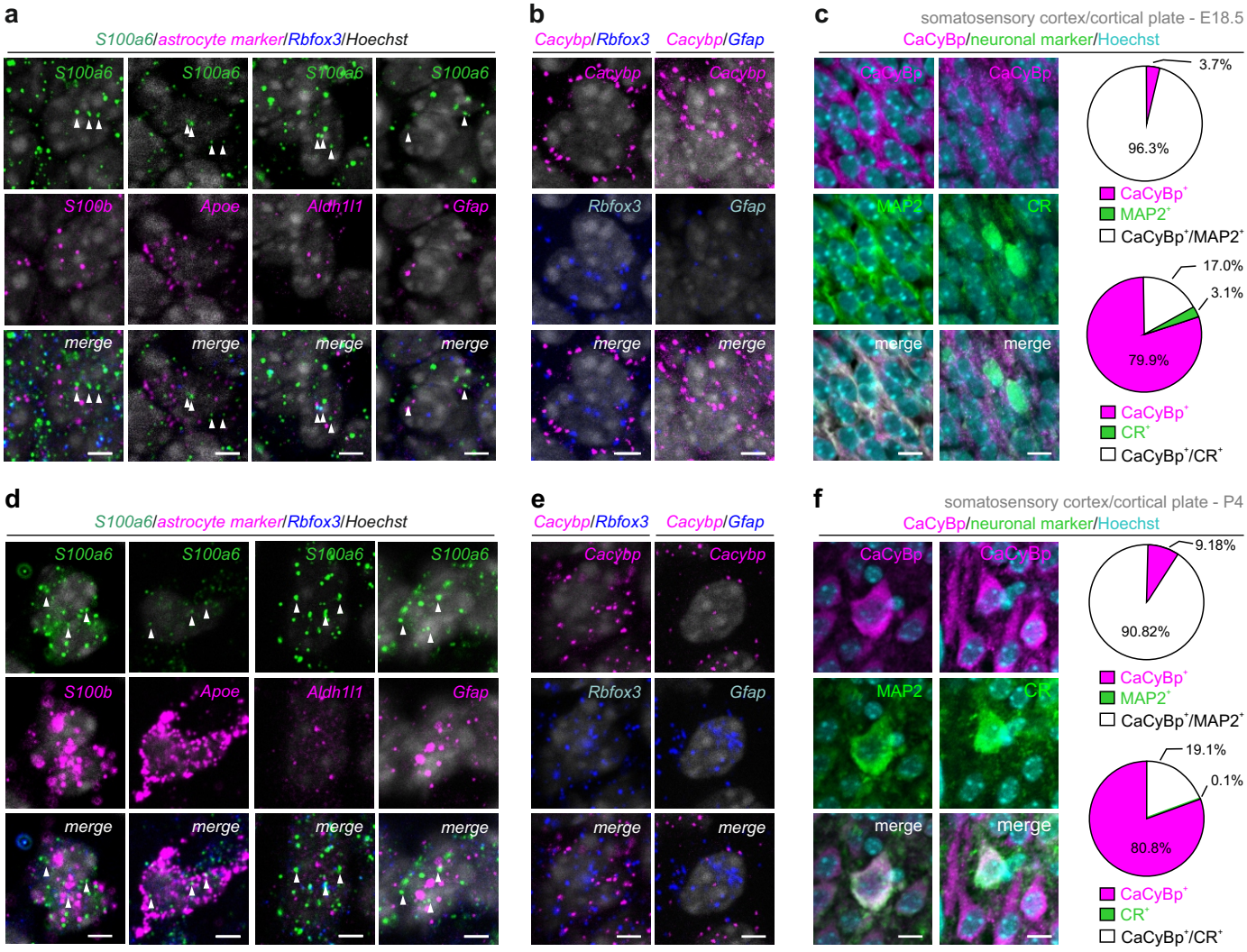

Cinquina *et al*. - Figure 3 (revised manuscript)

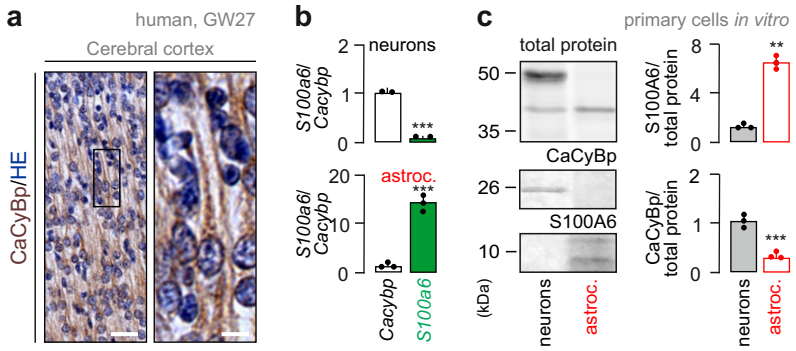

Cinquina *et al*. - Figure 4 (revised manuscript)

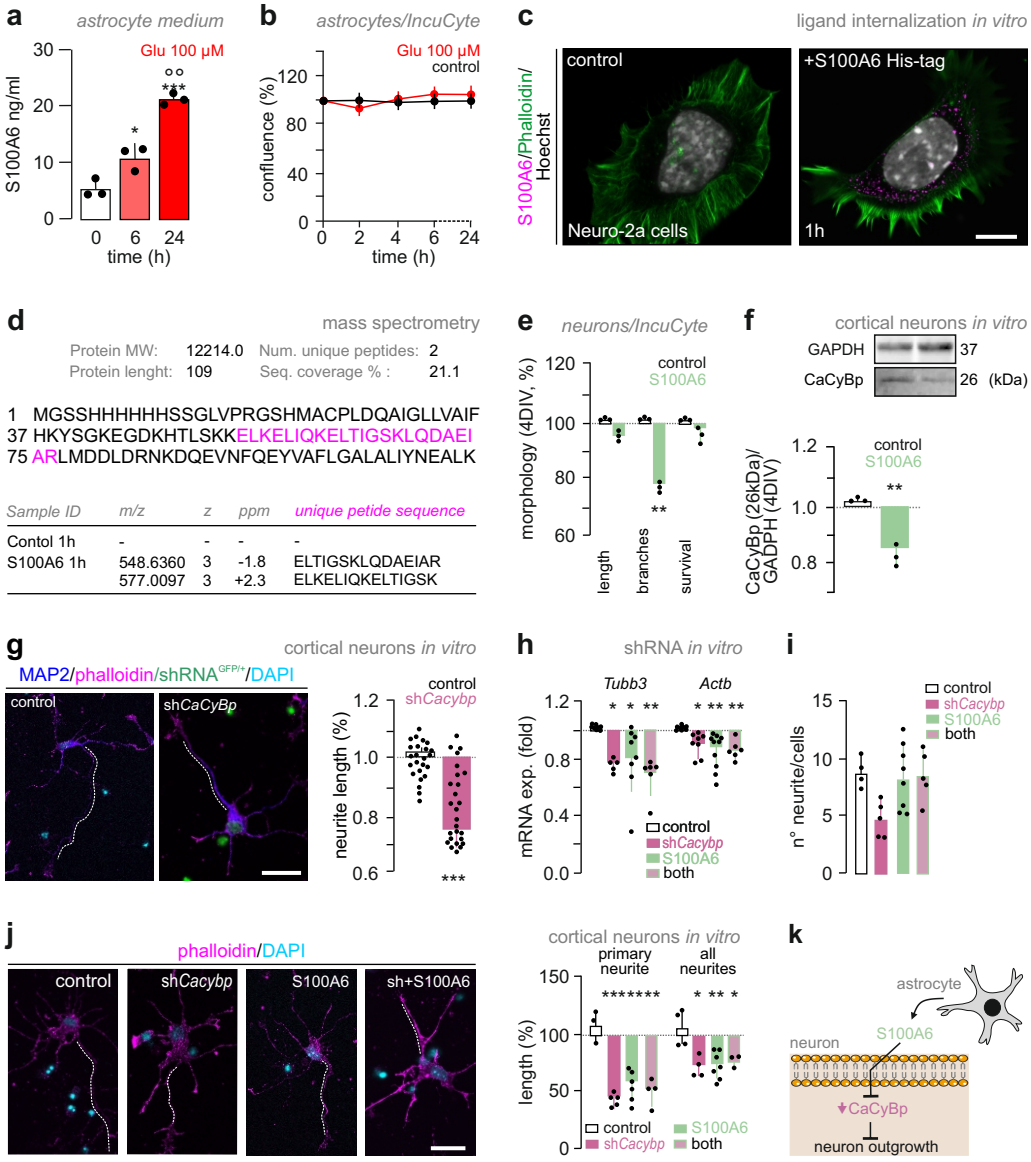

Cinquina *et al.* - Figure 5 (revised manuscript)

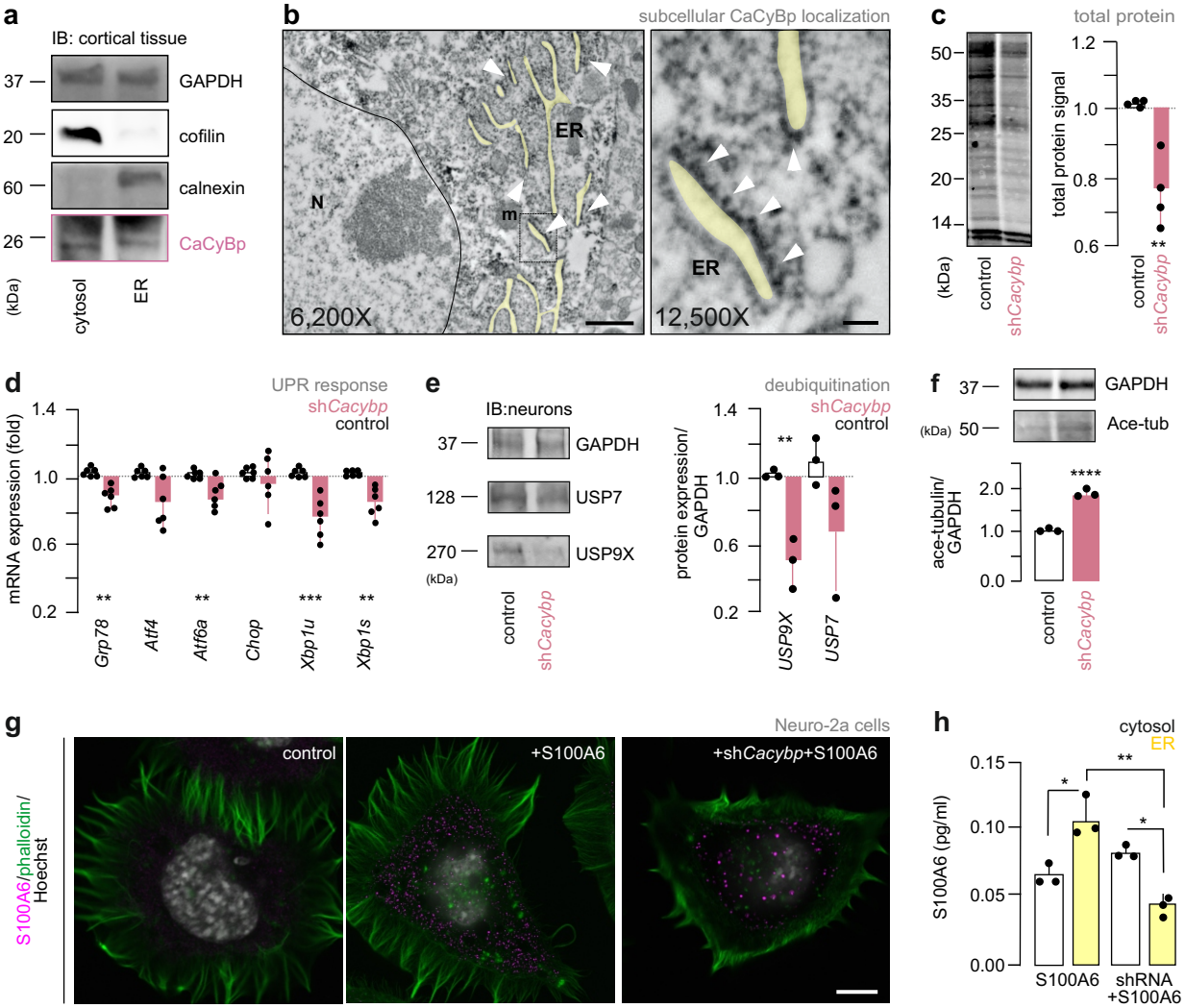

Cinquina *et al*. - Figure 6 (revised manuscript)

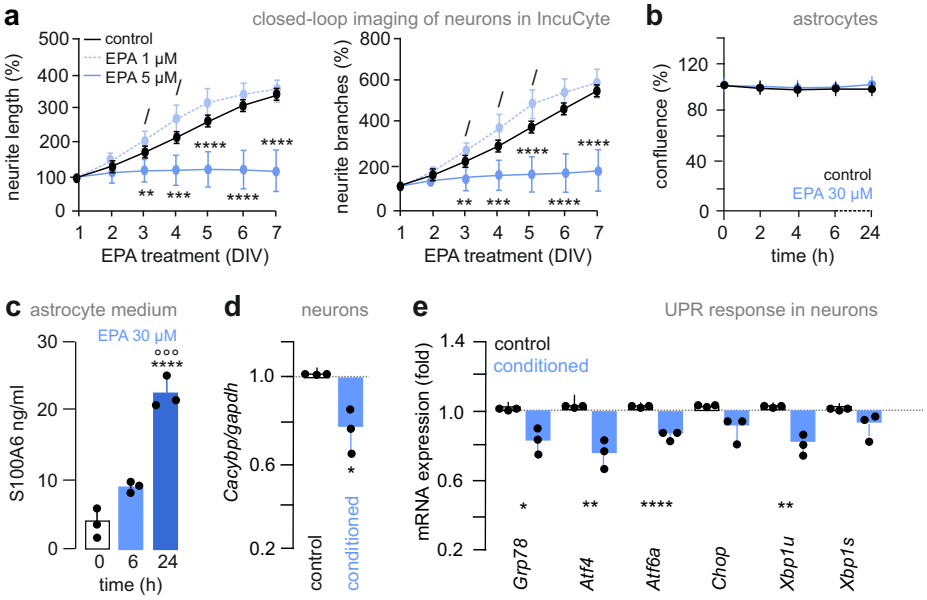

Cinquina *et al*. - Figure 7 (revised manuscript)

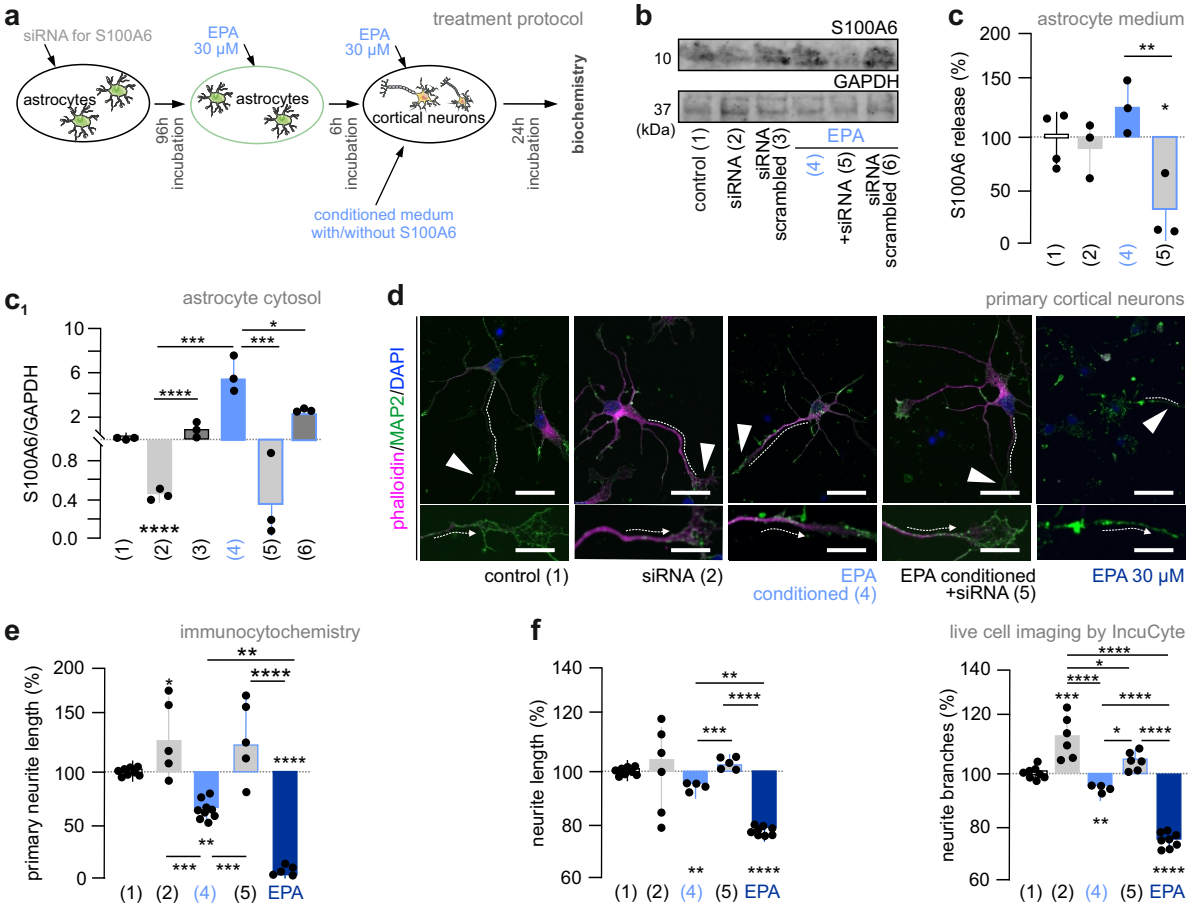
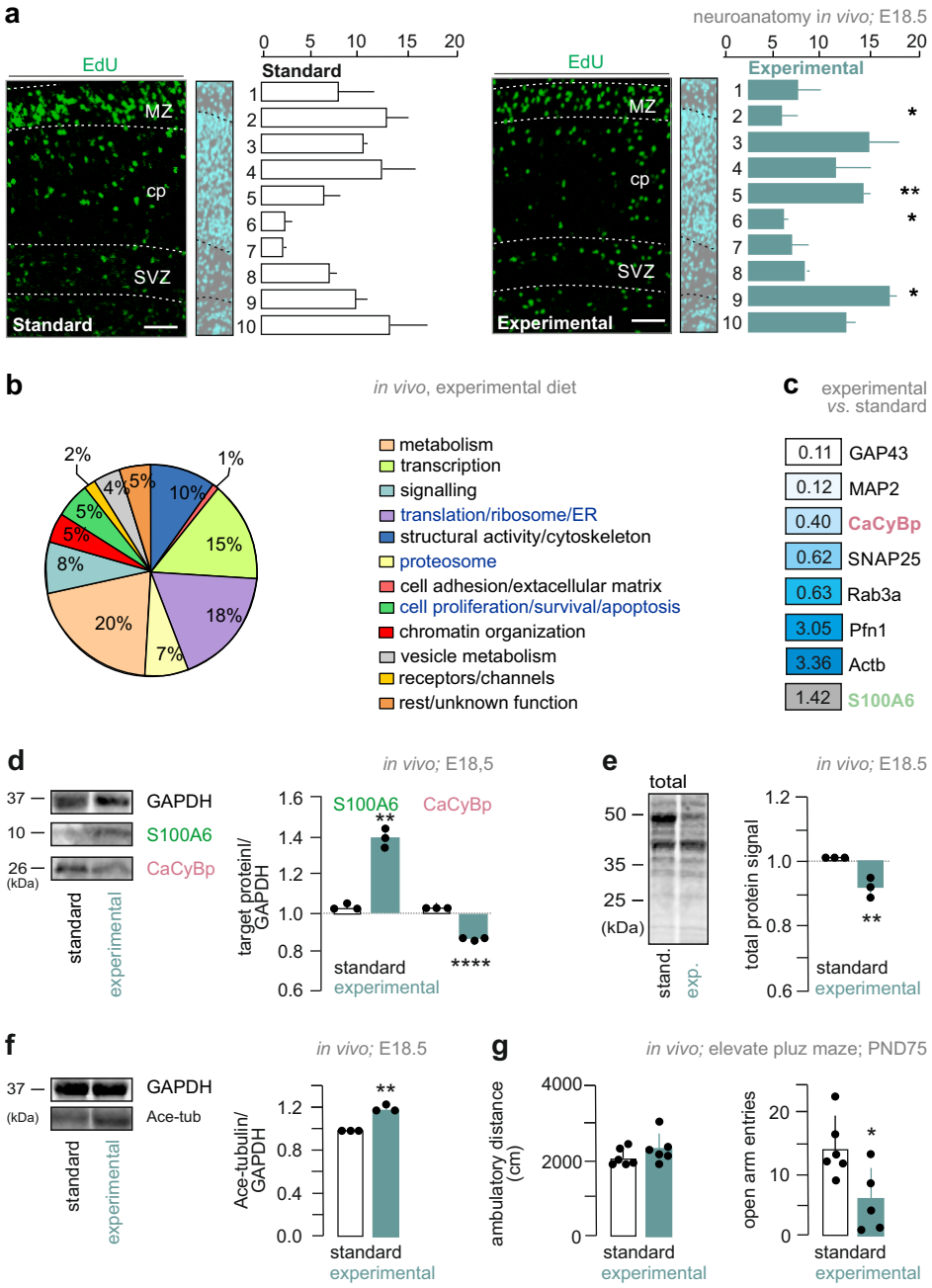
Cinquina *et al*. - Figure 8 (revised manuscript)